

**SCHOOL OF MATERIALS AND MINERAL RESOURCES ENGINEERING  
UNIVERSITI SAINS MALAYSIA**

**MULTI-DOPING OF Mg-Co SUBSTITUTED CARBONATED  
HYDROXYAPATITE FOR BIOMEDICAL APPLICATIONS**

By

**SYAHIDAH SUHAILI BT YAHAYA**

**SUPERVISOR: DR. YANNY MARLIANA BT BABA ISMAIL**

**CO-SUPERVISOR: PROF. DR. AHMAD FAUZI B MOHD NOOR**

Dissertation submitted in partial fulfillment of the requirements for the degree of  
Bachelor of Engineering with Honours  
(Materials Engineering)

Universiti Sains Malaysia

**JULY 2017**

## DECLARATION

I hereby declare that I have conducted, completed the research work and written the dissertation entitled **“Multi-Doping of Mg-Co Substituted Carbonated Hydroxyapatite for Biomedical Applications”**. I also declare that it has not been previously submitted for the award of any degree or diploma or other similar title of this for any other examining body or university.

Name of Student : Syahidah Suhaili bt Yahaya

Signature:

Date : 4<sup>th</sup> July 2017

Witnessed by

Supervisor : Dr Yanny Marliana bt Baba Ismail

Signature:

Date : 4<sup>th</sup> July 2017

## ACKNOWLEDGEMENTS

Bismillahirrahmanirrahim. Alhamdulillah and all praises to Allah S.W.T for giving me the strength and courage to successfully complete this project.

First and foremost, would like to thank Dr Yanny Marliana bt Baba Ismail, my supervisor and Prof Dr Ahmad Fauzi b Mohd Noor, my co-supervisor for their constant assistance and encouragement throughout the project. I am deeply grateful to their support from the very beginning to this day.

I also very grateful towards the technical staffs of School of Materials and Mineral Resources Engineering for helping me by providing lots of facilities, equipment and advices during my completion of the project.

My sincere thanks goes to Prof Fauzi's research team, Mr Iliya, Mr Hussein and Miss Myat Myat who had been given guidance in order for me to understand better in my study. I am indebted to them for their help.

Moreover, gratitude to Universiti Sains Malaysia for giving me the opportunity to seek knowledge, widen my experiences, explore my talents and have better preparation during my past four years of study.

My parents, Mr. Yahaya b Kasim and Mrs. Mahani bt Rawi deserve special mention for their inspiration, generous support and uncountable prayers. Thank you for the unconditional love.

Finally, I would like to thank to those who have contributed and involved directly or indirectly until my project has been successful.

# TABLE OF CONTENTS

<b>Contents</b>	<b>Page</b>
<b>DECLARATION.....</b>	<b>ii</b>
<b>ACKNOWLEDGEMENTS.....</b>	<b>iii</b>
<b>TABLE OF CONTENTS.....</b>	<b>iv</b>
<b>LIST OF TABLES .....</b>	<b>ix</b>
<b>LIST OF FIGURES .....</b>	<b>xi</b>
<b>LIST OF ABBREVIATIONS.....</b>	<b>xiii</b>
<b>LIST OF SYMBOLS.....</b>	<b>xiv</b>
<b>ABSTRAK .....</b>	<b>xv</b>
<b>ABSTRACT .....</b>	<b>xvi</b>
<b>CHAPTER 1.....</b>	<b>1</b>
<b>INTRODUCTION.....</b>	<b>1</b>
1.1    Research Background.....	1
1.2    Problem Statement.....	3
1.3    Objectives .....	4
1.4    Scope of Works .....	5
1.5    Outline of Chapters.....	6

<b>CHAPTER 2.....</b>	<b>7</b>
<b>LITERATURE REVIEW.....</b>	<b>7</b>
2.1 Introduction .....	7
2.2 Native Bone .....	7
2.2.1 Types of bone.....	8
2.2.2 Bone composition.....	10
2.2.3 Mechanical Properties of Native Bone .....	11
2.2.4 Bone’s Problem.....	13
2.3 Bone Graft Substitution.....	13
2.3.1 Autografts Bone Substitution.....	13
2.3.2 Allografts Bone Substitution.....	14
2.3.3 Xenografts Bone Substitution .....	14
2.4 Biomaterials.....	15
2.4.1 Definition of Biomaterials.....	15
2.4.2 Generation of Biomaterials .....	16
2.4.3 Properties of Biomaterials.....	17
2.5 Bioceramics .....	19
2.5.1 Introduction to Bioceramics .....	19
2.5.2 Classification of Bioceramics .....	19
2.6 Calcium Phosphate Bioceramics .....	20
2.6.1 Calcium phosphate .....	20
2.6.2 Hydroxyapatite .....	22

2.6.3	Limitation of Hydroxyapatite.....	23
2.6.4	Ionic Substitution in Hydroxyapatite .....	24
2.6.4.1	Anionic Substitutions .....	25
2.6.4.2	Cationic Substitutions.....	26
2.7	Synthesis of Hydroxyapatite Based Powders .....	27
2.8	Apatite Layer Formation .....	29
<b>CHAPTER 3.....</b>		<b>30</b>
<b>MATERIALS AND METHODOLOGY.....</b>		<b>30</b>
3.1	Introduction .....	30
3.2	Synthesis of CHA and Multi-Doped CHA Powders .....	31
3.2.1	Materials.....	31
3.2.2	Methodology .....	32
3.3	Fabrication of Dense CHA and Multi-Doped CHA .....	36
3.4	Sintering of CHA and Multi-Doped CHA.....	37
3.5	Bioactivity Test .....	37
3.5.1	Materials.....	37
3.5.2	Methodology .....	38
3.6	Characterization Techniques .....	40
3.6.1	X-Ray Diffraction .....	41
3.6.2	Fourier Transform Infra-Red Spectroscopy .....	42

3.6.3	Carbon, Hydrogen, Nitrogen Analyzer .....	42
3.6.4	X-Ray Fluorescence .....	42
3.6.5	Field Emission Scanning Electron Microscopy/Energy Dispersive X-Ray .....	43
3.6.6	Linear Shrinkage Measurement .....	43
3.6.7	Density and Porosity Measurement .....	44
3.6.7.1	Density of Powders.....	44
3.6.7.2	Apparent Porosity, Bulk Density and Apparent Density of Sintered Pellets .....	44
3.6.8	Diametral Tensile Strength .....	45
<b>CHAPTER 4.....</b>		<b>47</b>
<b>RESULTS AND DISCUSSION .....</b>		<b>47</b>
4.1	Introduction .....	47
4.2	Synthesis of Carbonated Hydroxyapatite .....	47
4.2.1	X-Ray Diffraction .....	48
4.2.2	Fourier Transform Infra-Red Analysis.....	50
4.2.3	Carbon, Hydrogen, Nitrogen Analysis.....	52
4.2.4	X-Ray Fluorescence Analysis .....	52
4.2.5	Field Emission Scanning Electron Microscopy/ Energy Dispersive X-Ray .....	53
4.3	Synthesis of Multi-Doped CHA Powders .....	56

4.3.1	X-Ray Diffraction .....	56
4.3.2	Fourier Transform Infra-Red Spectroscopy .....	58
4.3.3	Carbon, Hydrogen, Nitrogen Analyzer .....	59
4.3.4	X-Ray Fluorescence .....	60
4.3.5	Field Emission Scanning Electron Microscopy/ Energy Dispersive X-Ray .....	61
4.4	Fabrication of Dense Multi-Doped CHA .....	65
4.4.1	X-Ray Diffractions .....	65
4.4.2	Fourier Transform Infra-Red Spectroscopy .....	70
4.4.3	Linear Shrinkage Measurement .....	71
4.4.4	Density and Porosity Measurement .....	74
4.4.5	Diametral Tensile Strength .....	76
4.4.6	Field Emission Scanning Electron Microscopy/ Energy Dispersive X-Ray .....	77
<b>CHAPTER 5 .....</b>		<b>81</b>
<b>CONCLUSION AND RECOMMENDATION .....</b>		<b>81</b>
5.1	Conclusion .....	81
5.2	Recommendation for Future Work .....	82
<b>REFERENCES .....</b>		<b>83</b>

## LIST OF TABLES

	<b>Page</b>
<b>Table 2.1:</b> Mechanical properties of cortical bone and cancellous bone .....	10
<b>Table 2.2:</b> Composition of native bone .....	11
<b>Table 2.3:</b> Mechanical properties of human cortical bone .....	12
<b>Table 2.4:</b> Three generations of biomaterials .....	17
<b>Table 2.5:</b> Important properties for biomaterials .....	18
<b>Table 2.6:</b> Properties of biologically relevant calcium phosphates .....	21
<b>Table 2.7:</b> Mechanical properties of native bone tissue and hydroxyapatite .....	22
<b>Table 2.8:</b> Type of methods used to synthesize HA nanoparticles .....	28
<b>Table 3.1:</b> List of raw materials used in nanoemulsion method and their function .....	31
<b>Table 3.2:</b> Composition of mineral phase in bone .....	35
<b>Table 3.3:</b> Composition of magnesium and cobalt in each sample .....	36
<b>Table 3.4:</b> List of raw materials used to prepare 1000 ml SBF solution .....	38
<b>Table 4.1:</b> Data obtained by XRD analysis .....	50
<b>Table 4.2:</b> List of wave number for carbonate band to classify an A-type CHA and B-type CHA .....	51
<b>Table 4.3:</b> Typical bands of HA pattern according to its functional groups .....	52
<b>Table 4.4:</b> Amount of carbon and carbonate content in CHA powders .....	52
<b>Table 4.5:</b> XRF results of CHA powder without doping .....	53
<b>Table 4.6:</b> EDX results of CHA powder taken at three preferred points of sample .....	55
<b>Table 4.7:</b> XRD data of as-synthesized multi-doped CHA powders .....	58
<b>Table 4.8:</b> Amount of carbon and carbonate content in CHA and multi-doped CHA ..	60
<b>Table 4.9:</b> XRF results of as-synthesized multi-doped CHA .....	61

<b>Table 4.10:</b> EDX results for the as-synthesized multi-doped CHA, (a)Mg-Co CHA 1, (b) Mg-Co CHA 2, (c) Mg-Co CHA 3 and (d) Mg-Co CHA 4 .....	63
<b>Table 4.11:</b> XRD data of sintered dense CHA .....	68
<b>Table 4.12:</b> XRD data of sintered dense multi-doped CHA . .....	69
<b>Table 4.13:</b> Average diameter, average thickness and percent of shrinkage for (a) Diameter and (b) Thickness of CHA .....	72
<b>Table 4.14:</b> Average diameter and percent of diameter shrinkage for (a) Mg-Co CHA 1 and (b) Mg-Co CHA 2 .....	73
<b>Table 4.15:</b> Average thickness and percent of thickness shrinkage for (a) Mg-Co CHA 1 and (b) Mg-Co CHA 2 .....	73
<b>Table 4.16:</b> Average apparent porosity, bulk density, powder density and relative density for (a) CHA (b) Mg-Co CHA 1 and (c) Mg-Co CHA 2 .....	75
<b>Table 4.17:</b> Tensile strength of sintered CHA and multi-doped CHA .....	77

## LIST OF FIGURES

	<b>Page</b>
<b>Figure 1.1:</b> Flowchart of the summarized overall research flow .....	5
<b>Figure 2.1:</b> Structural organization in a human long bone .....	8
<b>Figure 2.2:</b> Cross sectional of human bone .....	9
<b>Figure 2.3:</b> Phase present in human bone .....	10
<b>Figure 2.4:</b> Long bone development which undergo both osteogenesis and angiogenesis process .....	23
<b>Figure 2.5:</b> HA structure from c-axis point of view. Black lines connect Ca(I) columns in hexagonal networks. Cyan and magenta triangles connect staggered Ca(II) atoms lying in the same plane, but at different height with respect to the c-axis .....	24
<b>Figure 2.6:</b> Apatite layer that formed on the surface of sample after being soaked in SBF solution .....	29
<b>Figure 3.1:</b> Process flow to synthesis CHA powders as reference powders .....	33
<b>Figure 3.2:</b> Process flow to synthesis multi-doped CHA powder.....	34
<b>Figure 3.3:</b> Sintering profile for sintering process .....	37
<b>Figure 3.4:</b> Setup of apparatus for SBF solution preparation .....	39
<b>Figure 3.5:</b> Schematic diagram of specimen immersed in SBF solution.....	40
<b>Figure 3.6:</b> Classification of characterization techniques used in this study .....	41
<b>Figure 3.7:</b> Schematic diagram of Diametral Tensile Strength (DTS) test.....	46
<b>Figure 4.1:</b> (a) XRD pattern of CHA based powders without doping that matched with (b) reference pattern of HA.....	49
<b>Figure 4.2:</b> FTIR spectra of as-synthesized CHA powders . .....	51
<b>Figure 4.3:</b> Surface morphology of as-synthesized CHA powders .....	54
<b>Figure 4.4:</b> Actual EDX results of CHA powders taken at preferred points . .....	55

<b>Figure 4.5:</b> XRD pattern of as-synthesized multi-doped CHA powders .	57
<b>Figure 4.6:</b> FTIR spectra of the as-synthesized multi-doped CHA powders compared with CHA powders. (a) CHA, (b) Mg-Co CHA 1, (c) Mg-Co CHA 2, (d) Mg-Co CHA 3 and (e) Mg-Co CHA 4	59
<b>Figure 4.7:</b> Surface morphology of the as-synthesized multi-doped CHA powders. (a) Mg-Co1, (b) Mg-Co2, (c) Mg-Co3 and (d) Mg-Co4	62
<b>Figure 4.8:</b> (a) XRD pattern of sintered pure CHA which comply with (b) HA reference pattern .	66
<b>Figure 4.9:</b> Comparison of XRD pattern between pure CHA before sintering and after sintering	67
<b>Figure 4.10:</b> XRD pattern of sintered multi-doped CHA pellets	69
<b>Figure 4.11:</b> FTIR spectra of sintered CHA based without doping	70
<b>Figure 4.12:</b> FTIR spectra of sintered multi-doped CHA compared with CHA based. (a) CHA based, (b) Mg-Co CHA 1 and (c) Mg-Co CHA 2	71
<b>Figure 4.13:</b> Percent of shrinkage in diameter and thickness of CHA, Mg-Co CHA 1 and Mg-Co CHA2	74
<b>Figure 4.14:</b> Relative density of CHA and multi-doped CHA	76
<b>Figure 4.15:</b> Surface morphology of CHA based under 5000x and 10000x magnification	78
<b>Figure 4.16:</b> Surface morphology of Mg-Co CHA1 based under (a) 5000x and (b) 10000x magnification .	78
<b>Figure 4.17:</b> Surface morphology of Mg-Co CHA2 based under (a) 5000x and (b) 10000x magnification .	78
<b>Figure 4.18:</b> EDX result of (a) CHA (b) Mg-Co CHA 1 (c) Mg-Co CHA 2	80

## LIST OF ABBREVIATIONS

CHA	Carbonated Hydroxyapatite
CHN	Carbon, Hydrogen and Nitrogen
DTS	Diametral Tensile Strength
EDX	Energy Dispersive X-Ray
FESEM	Field emission scanning electron microscope
FTIR	Fourier Transform Infra-Red
FWHM	Full width at half maximum
HA	Hydroxyapatite
ICDD	International Centre for Diffraction Data
Min	Minute
mm	Millimeter
nm	Nanometer
Pa	Pascal
SBF	Simulated Body Fluid
SEM	Scanning electronic microscopy
T	Temperature
XRD	X-Ray diffraction

## LIST OF SYMBOLS

Å	Armstrong
°	Degree
°C	Degree Celsius
M	Mega
μ	Micro
%	Percentage
λ	Wavelength
wt%	Weight percent

# **PELBAGAI PENGEDOPAN Mg-Co DIGANTI HIDROKSIAPATIT TERKARBONAT UNTUK KEGUNAAN BIOPERUBATAN**

## **ABSTRAK**

Hidroksiapatit terkarbonat ialah biobahan yang menjanjikan kesesuaian untuk digunakan sebagai tulang gantian. Walau bagaimanapun, dalam hidroksiapatit terkarbonat terdapat limitasi, yang mana hidroksiapatit terkarbonat mempunyai kestabilan haba yang rendah. Oleh itu, kajian ini dijalankan untuk mengkaji kesan hidroksiapatit terkarbonat pelbagai pengedopan melalui analisis kimia, mekanikal, fizikal dan biologi. Pelbagai pengedopan hidroksiapatit terkarbonat telah berjaya disintesis melalui kaedah pengemulsion nano, melalui teknik mencurah langsung dalam kajian ini diikuti dengan pencirian serbuk yang terhasil. Analisa mendapati bahawa Mg-Co CHA 1 dan Mg-Co CHA 2 mempunyai komposisi optimum. Serbuk yang dihasilkan adalah jenis B hidroksiapatit terkarbonat. Serbuk ini kemudiannya difabrikasi melalui kaedah mempatan kering dan disinter pada suhu 900°C. Gas karbon dioksida kering telah dibekalkan kepada sampel selepas disejukkan kepada 200°C untuk mengimbangi penguraian karbonat semasa pensinteran. Penggunaan gas karbon dioksida kering telah berjaya mengimbangi karbonat yang terurai semasa pensinteran. Sample yang disinter kekal sebagai jenis B hidroksiapatit terkarbonat. Ujian bioaktiviti *in vitro* juga telah dijalankan untuk sampel pelbagai pengedopan hidroksiapatit terkarbonat tersinter selama tujuh hari. Hasil analisa SEM untuk pelbagai pengedopan hidroksiapatit terkarbonat selepas tujuh hari menunjukkan bahawa lapisan apatit telah berjaya terbentuk untuk semua komposisi. Oleh itu, komposisi optimum yang menghasilkan jumlah lapisan apatit yang tinggi, sifat mekanik dan fizikal adalah Mg-Co CHA 2, yang mana magnesium dalam jumlah maksimum dan kobalt dalam jumlah minimum.

# MULTI-DOPING OF Mg-Co SUBSTITUTED CARBONATED HYDROXYAPATITE FOR BIOMEDICAL APPLICATIONS

## ABSTRACT

Carbonated hydroxyapatite (CHA) is a promising biomaterials that is suitable to be used as bone substitution. However, CHA has limitation, as it has low thermal stability. Thus, this study was conducted to investigate the effect of multi-doped CHA through chemical, mechanical, physical and biological analysis. Multi-doped CHA was successfully synthesis via nanoemulsion method, through direct pouring technique, followed by characterizations of the produced powders. It was found that Mg-Co CHA 1 and Mg-Co CHA 2 had the optimum compositions. The powders produced were B-type CHA. These powders were then fabricated by dry pressing method and sintered at 900°C. Dry carbon dioxide (CO<sub>2</sub>) gas was supplied to the sample after cooled down to 200°C to compensate carbonate decomposition during sintering. Used of dry CO<sub>2</sub> had successfully compensate the carbonate decomposition during sintering. The sintered samples were maintained as B-type CHA. *In vitro* bioactivity test also was done for sintered multi-doped CHA for seven days. SEM observation for dense multi-doped CHA after seven days showed that apatite layer were successfully formed for all compositions. Thus, the optimum composition that produced high amount of apatite layer, good chemical, mechanical and physical properties is Mg-Co CHA 2, where magnesium in maximum amount and cobalt in minimum amount.

# CHAPTER 1

## INTRODUCTION

### 1.1 Research Background

Bone is a rigid organ in skeleton system of human body that plays an important role to support the body weight, enable us to move, safeguard the other organ from external injury and generate red and white blood cells (Wu, 2010). There are 206 bones in an adult human body which can be classified into two types, cortical bone and cancellous bone. Cortical bone also known as compact bone that has low porosity, while cancellous bone also known as spongy bone which has high porosity.

Incident, disease, bone fracture and obesity may lead to bone failures. In 2015 only, demand for bone grafts in US market had reach up to \$3.18 billion. Particularly, bone defects were cured using various medical surgical techniques, such as, autograft, allograft and replacement implant (Bandyopadhyay et al., 2006). Autograft is a bone transplantation from one part of the body to another of the same patient, while allograft is a bone transplantation from one individual to another with same species as the recipient, without genetically identical. Replacement implantation is bone transplantation by using prosthetic materials to replace the injured tissue, in which is a popular choice and well known (Wu, 2010). Even though bone grafting had cured many cases, this method are still facing with an issue and disadvantage, as this method has limited lifespan, have side effect, which may cause an inflammation and could not withstand mechanical forces when being tested via *in vivo* testing and produce weakly organized sheets of cells. Thus, it is important to produce bone grafting materials that allowed rapid cell growth and restore the use of bone as functional load bearing that could withstand mechanical forces for ambulatory function (Bandyopadhyay et al., 2006).

As for alternative to replace bone graft applications, synthetic biomaterials were introduced as new substituting materials to assist the healing process of the bone injury by generate bone growth. There are three classes of materials for biomaterials, which are ceramic, metal and polymer. As for this study, ceramic biomaterials was the main focus, where hydroxyapatite is the most frequent used materials in biomedical applications (Teixeira et al., 2010).

Human bone made of various phases, the main phase of bone are water, collagen polymer phase and inorganic phase. Inorganic phase of bone made of calcium phosphate based with the presence of other trace elements such as  $\text{Na}^+$ ,  $\text{Mg}^{2+}$ ,  $\text{K}^+$  and  $\text{F}^-$ . Calcium phosphate is a natural occurring bone mineral which is bio-active, bio-resorbable and osteoconductive. Calcium phosphate have various classifications, which are classified based of the ratio of calcium to phosphate (Ca/P) (Bandyopadhyay et al. 2006). Hydroxyapatite (HA) is a calcium phosphates based with ratio 1.67. HA is a well-known biomaterials that has similarity to the bone mineral component and frequently used for bone substitute applications (Shepherd et al., 2012). HA is suitable to be used as biomedical applications as it is biocompatible and osteoconductive.

The presence of other trace elements such like magnesium for an example, give an influence to the performance of bone (Bandyopadhyay et al., 2006). In order to nearly mimic bone mineral composition, numerous substitutions have been done, both cationic and anionic substitutions. Cationic substitutions have been done by substituting an ions into calcium sites, while anionic substitutions was done by substituting an ions into phosphate or hydroxyl sites for HA (Shepherd et al., 2012). It is important to incorporate these trace elements into implants because the biocompatibility of apatite is closely dependent on their composition (Bandyopadhyay et al., 2006).

As for this study, cationic substitutions have been done by substituting magnesium and cobalt ions into calcium sites, while anionic substitutions was done by substituting carbonate ions into phosphate sites for HA. Carbonate ions is the most abundant ions that present in bone, which range from 4 to 8wt%. Substitution of carbonate ions into HA structure improved the biological activity compared to pure HA, as incorporation of carbonate ions into HA caused a change in crystal morphology, decrease in crystallinity, increase in solubility and increase the local concentration of calcium and phosphate ions that are necessary for new bone formation (Kumar et al. 2012). While, substitution of magnesium ions in HA structure stimulate the angiogenesis, which is blood vessel formation properties and improve bioactivity compare to pure HA (Laurencin et al. 2011). The substitution of cobalt ions in HA structure as it stimulate the angiogenesis properties, which is the blood vessel formation process and improve the bioactivity, physical, chemical and mechanical properties compare to pure HA (Kulanthaivel et al. 2015).

## **1.2 Problem Statement**

Hydroxyapatite (HA) has been widely used in bone repair and regeneration. However, HA has a limited bioactivity, even though it is biocompatible and osteoconductive. This is due to its stability that lead to enormously slow degradation rate in biological fluids. The solubility properties closely related to the chemical reaction with other compound and its biocompatibility with tissue (Mickiewicz, 2001).

Moreover, mineral in bone is not solely stoichiometric HA, but also contains minor substituents such as carbonate, sodium, magnesium and other elements. Among the substituting ions, the present study focuses on carbonate substituted into HA structure which exists in the bone at about 4-8 wt% and transmit solubility to bone. Hence the apatite forming ability of CHA will nearly mimic the natural bone mineralization

(Parthiban et al., 2011). However, carbonate has lower thermal stability where it starts to decompose at 800°C in normal sintering atmosphere (air) (Barinov et al., 2006). In general, higher sintering temperatures are required to produce highly densified products in order to obtain good mechanical properties.

Therefore, the aim of this project is to produce dense multi-doped CHA with good physical, mechanical and biological properties. In this study, the introduction of magnesium and cobalt ions into the CHA structure are hoped to enhance the biological activity and closely mimic the bone mineral. While, the introduction of dry carbon dioxide (CO<sub>2</sub>) after sintering is hoped to compensate carbonate loss due to decomposition during sintering process. It is also hoped that the dense multi-doped CHA formed were chemically, biologically, mechanically and structurally similar to human bone mineral.

### 1.3 Objectives

The aim of this research is to produce multi-doped carbonated hydroxyapatite (CHA) with good physical, mechanical and biological properties in order to mimic the human bone mineral. Therefore, the following objectives are set:

- 1) To produce a range of magnesium and cobalt co-substituted Carbonate Hydroxyapatite (CHA) nanopowders via nanoemulsion techniques.
- 2) To characterize the as-synthesized multi-doped Carbonate Hydroxyapatite (CHA) nanopowders physically and chemically/elementally.
- 3) To fabricate dense multi-doped Carbonate Hydroxyapatite (CHA).
- 4) To investigate the *in vitro* activity and mechanical properties of the fabricated dense multi-doped Carbonate Hydroxyapatite (CHA).

## 1.4 Scope of Works

In general, this work can be divided into four main parts. Synthesis of CHA and multi-doped CHA powders were done in the first parts of this project, followed by characterization and finding of optimum as-synthesized powders. The final parts of this work was preparation of bulk dense via dry pressing method, which then sintered at 900°C CHA composition and followed by characterization sintered dense multi-doped CHA.

Figure 1.1 represents the flowchart for the scope of work involved in this study.

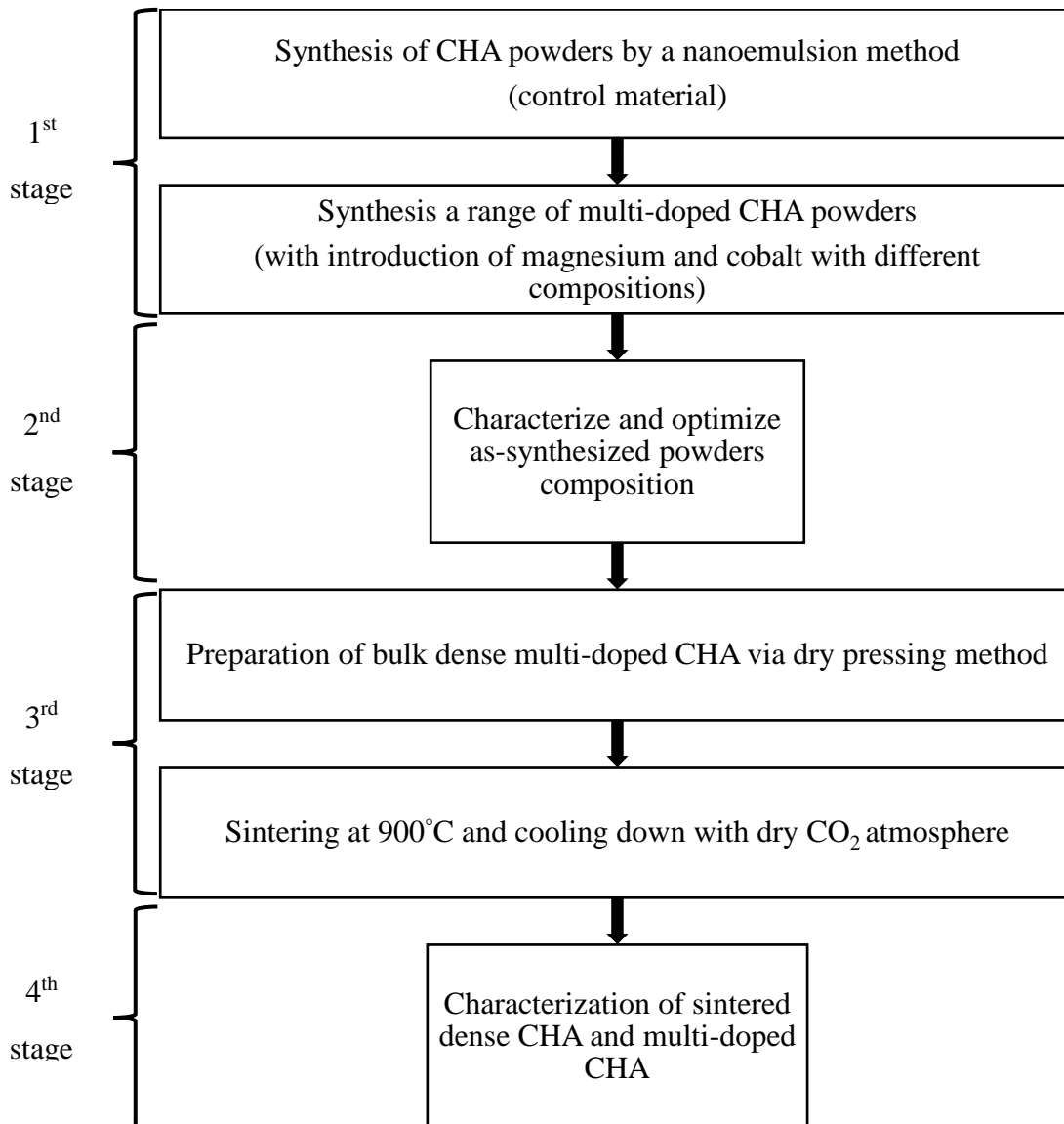


**Figure 1.1:** Flowchart of the summarized overall research flow.

## **1.5 Outline of Chapters**

There are five chapters in this thesis. Chapter one discusses on the introduction, problem statement, objectives, scope of work regarding the project. Meanwhile, concept, theory and literature review related to background and fabrication of multi-doped carbonated hydroxyapatite are explained in chapter two. In chapter three, experimental details and characterization techniques used are explained respectively. Then, chapter four focuses on the results and discussion of this project. Finally, conclusion and recommendations of future work are stated in chapter five.

## **CHAPTER 2**

### **LITERATURE REVIEW**

#### **2.1 Introduction**

In this chapter, a brief explanation about structure and properties of native bone, bone graft, biomaterials, bioceramics and calcium phosphate bioceramics were discussed to provide basic knowledge and an idea about this project. Furthermore, even though nanoemulsion was used to synthesis multi-doped Carbonated Hydroxyapatite (CHA) based powder and dry pressing method with sintering at 900°C were implemented to densify the ceramic body from powders, a brief overview regarding other method used by previous studies were also discussed in this study to compare each method used and their findings.

#### **2.2 Native Bone**

Native bone is a complex structure that played a very important role in human body, as it function to support human body, as well as protect the internal organ and store healing cells (Kehoe & Eng, 2008). It is important to understand the structure and properties of native bone in order to develop a new engineering biomaterials to heal bone fracture. A huge dissimilarity of new develop engineering biomaterials from host tissue may cause the objective of development could not be achieved, as well as give a negative effects to the host body tissue (Wang, 2003).

### 2.2.1 Types of bone

Native bone has several levels of structural organization which can be identified from macroscale to microscale. There are two levels of composite structure that can be considered while developing bone substituted. Firstly, the bone apatite reinforced collagen forms individual lamella in the scale of nm to mm. Then, the apatite-collagen composites at the microscopic level that provides the basis for producing bioactive ceramic-polymer composites as analogue biomaterials for bone replacement (Wang, 2003).

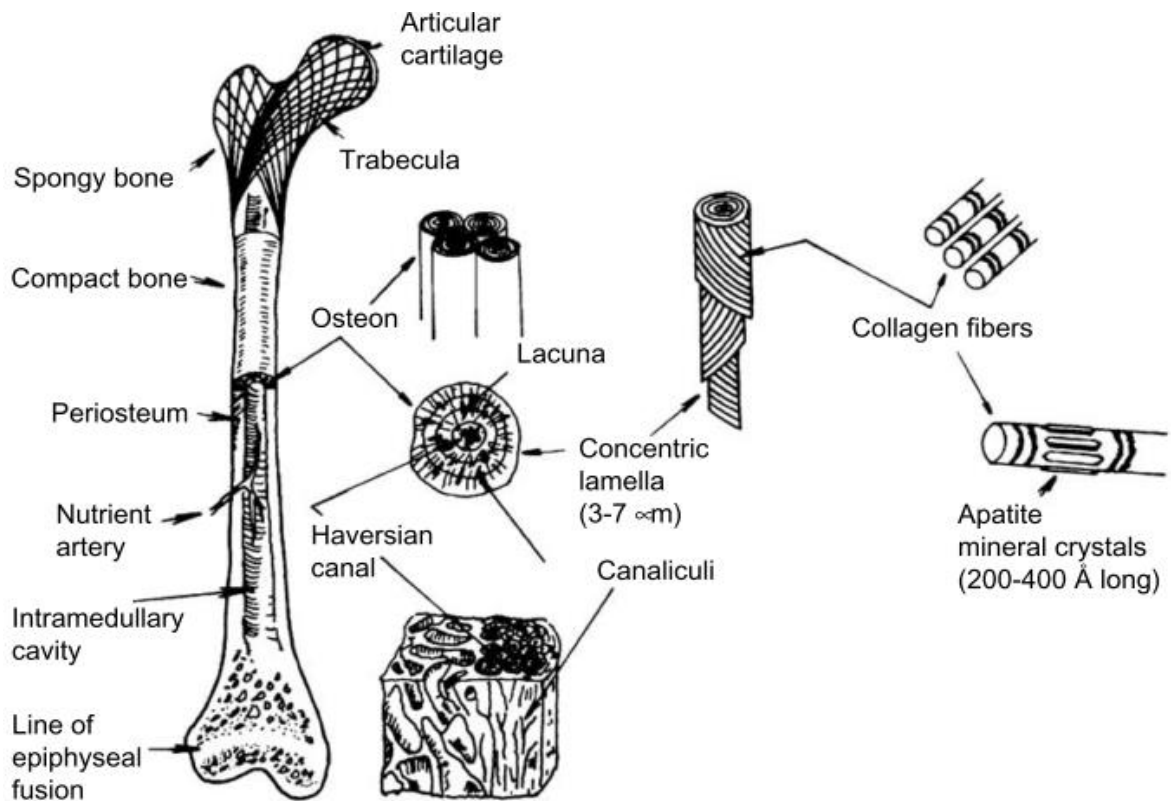


**Figure 2.1:** Structural organization in a human long bone (Wang, 2003).

There are two type of bone, which are cortical bone and cancellous bone. Bone structure can be classified into two parts based on its porosity, which are cortical bone and cancellous bone (Kehoe & Eng, 2008). Cortical bone is a dense bone with porosity

from 5% to 10%. Cortical bone forms at the external shell of the bone, with thickness up to several tenths of a millimetre to several millimeter or even centimeters. As for cancellous bone or also known as trabecular bone, it is a spongy bone with porosity from 75% to 95%. Cancellous bone forms in inner side of bones, with thickness about 50-300  $\mu\text{m}$ , with an orientation that depends on the load distribution in the bone (Eliaz & Metoki, 2017).

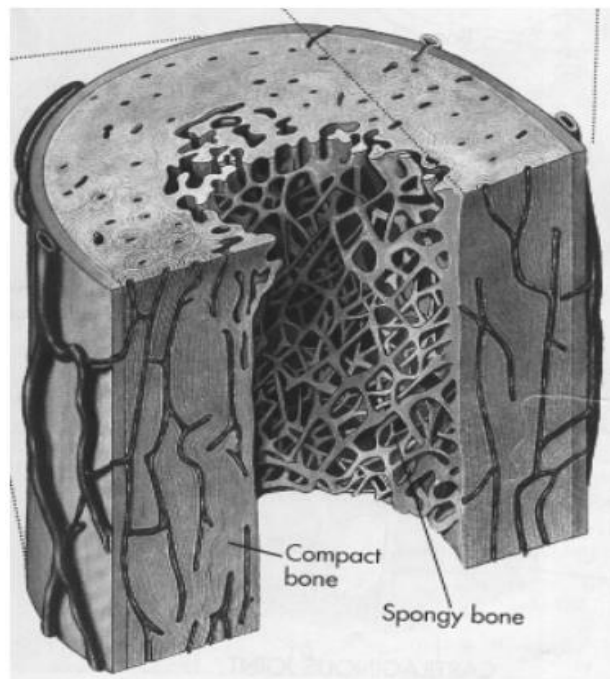


**Figure 2.2:** Cross sectional of human bone (Bandyopadhyay et al., 2006).

The percentage of porosity for both cortical and cancellous bone are very huge, thus this affect the mechanical properties of each bone. The different in term of Young's modulus, tensile strength, compressive strength and fracture toughness between cortical and cancellous bone are shown in Table 2.1 (Eliaz & Metoki, 2017).

**Table 2.1:** Mechanical properties of cortical bone and cancellous bone (Eliaz & Metoki, 2017).

	<b>Cortical Bone</b>	<b>Cancellous Bone</b>
<b>Young's Modulus</b>	7–30 GPa	50–500 MPa
<b>Tensile Strength</b>	50–150 MPa	1.2–20 MPa
<b>Compressive Strength</b>	167–193 MPa	1.9–10 MPa
<b>Fracture Toughness (K<sub>1c</sub>)</b>	2–12 MPa·m <sup>1/2</sup>	0.1 MPa·m <sup>1/2</sup>

### 2.2.2 Bone composition

Human bone composes of organic phase, inorganic phase, and water, where 65% of it are made up of inorganic phase, 25% made up of organic phase and remaining 10% made up of water (Kehoe & Eng, 2008). Inorganic phase of human bone consist of various bone minerals, where calcium phosphate as the main element. Besides, organic phase of human bone consists of 90% to 95% of collagen (Dorozhkin & Epple, 2002).

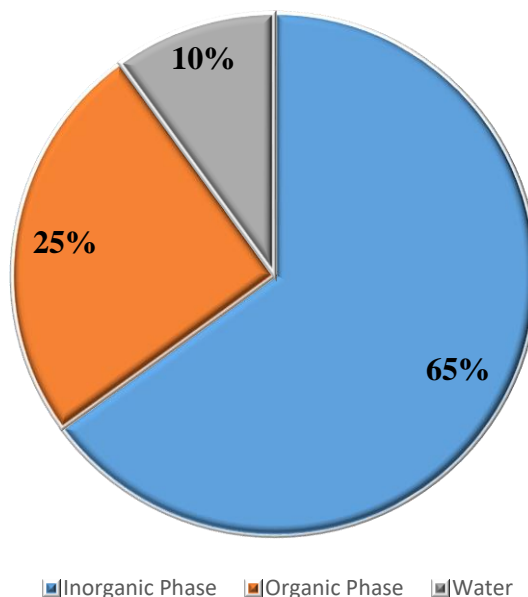


**Figure 2.3:** Phase present in human bone (Kehoe & Eng, 2008).

Calcium and phosphorus are the main elements in bone mineral composition with 25.4wt% and 11.6wt%. There are also small amount other element present in bone mineral composition, which listed in Table 2.2.

**Table 2.2:** Composition of native bone (Combes et al., 2016; Kehoe & Eng, 2008).

Elements	Chemical Formula	Bone composition (wt%)	
		Major Elements	
Calcium	Ca	25.4	
Phosphorus	P	11.6	
Carbonates	CO <sub>3</sub> <sup>2-</sup>	5.6	
Nitrogen	N	4.9	
Minor Elements			
Magnesium	Mg	0.27	
Sodium	Na	0.53	
Chloride	Cl	0.13	
Potassium	K	0.0047	
Sulphide	S	0.08	
Main Trace Elements			
Cobalt	Co	0 - 2.5×10 <sup>-6</sup>	
Zinc	Zn	0 – 3.9×10 <sup>-3</sup>	
Strontium	Sr	0 – 0.05	
Iron	Fe	7.6×10 <sup>-3</sup>	
Fluoride	F	0.04	
Aluminium	Al	2.9×10 <sup>-3</sup>	
Plumbum	Pb	4.4×10 <sup>-4</sup>	

### 2.2.3 Mechanical Properties of Native Bone

The mechanical properties of human bone have been studied in term of its tensile strength, compressive strength, Young’s modulus and fracture toughness. Cortical bone

and cancellous bone may have different value of mechanical properties. This is due to their variance in their structure, percentage of porosity and function. Mechanical properties of bone also are influenced by orientation of bone specimen, either it is longitudinal or transverse. Longitudinal is running parallel to the predominant osteon ligaments and transverse is through the osteon section (Kehoe & Eng, 2008).

**Table 2.3:** Mechanical properties of human cortical bone (Kehoe & Eng, 2008).

<b>Mechanical Properties</b>	<b>Test direction related to bone axis</b>	
	<b>Parellel</b>	<b>Normal</b>
<b>Tensile strength (MPa)</b>	124 – 174	49
<b>Compressive strength (MPa)</b>	170 – 193	133
<b>Young’s Modulus (GPa)</b>	17 – 18.9	11.5
<b>Fracture Toughness (MPa m<sup>1/2</sup>)</b>	2 - 12	8

In dense or cortical bone, its mechanical properties are influenced significantly by the percentage of porosity, mineralization level and the organization of the solid matrix. Previous study found that mechanical properties of cortical bone from the tibia, femur and humerus are differ between subjects, although the density remains the same. However, it is in contrast for cancellous bone, as there is no different in mechanical properties of the humerus, proximal tibia and lumbar spine (Kehoe & Eng, 2008).

#### **2.2.4 Bone's Problem**

Osteoporosis, arthritis and bone tumor are common diseases related to bone that lead to failure of bone and joint. Other than diseases, incidents, obesity, diabetes and ageing population also the driving force of failure of bone and joint. As a support of body weight, bone played an important role in our daily life. Thus, it is vital to seek for a replacement and repair for bone failure to preserve daily life style (Shepherd et al., 2012).

### **2.3 Bone Graft Substitution**

Bone replacement and repair is a huge global market. In the United States and England, there are around 1 million bone-grafting procedures take place annually on the pelvis, spine and other extremities with around 700,000 joint replacement surgeries taking place in a year (Shepherd et al., 2012).

Repairing bone defects involves various medical surgical treatments, for example of bone graft substitution, external fixation devices and electrical stimulation. Bone graft substitution is classified into three types, which are, autograft, allograft and xenograft are commonly known as effective treatments for bone replacement and regeneration (Whited et al., 2005).

#### **2.3.1 Autografts Bone Substitution**

Autografts or also known as autogenous bone grafting are bone graft substitution taken from another part of the patient's own body. Autografts had been an effective treatments for bone defects for years as it provides osteogenic cells as well as essential osteoinductive factors required for bone healing and regeneration. Trabecular bone from the patient's own iliac crest was the common used for bone healing and regeneration. In

addition, cortical bone also can be used depend on the defect size, shape and application. However, autografts bone substitution has limitation, where the volume of bone accessible to be used and concerns of donor site morbidity (Whited et al., 2005). The drawbacks of this method: also is that the patient has to endure two surgical interventions instead of one and there are general risks of infection such as HIV (Vallet-regí, 2010).

### **2.3.2 Allografts Bone Substitution**

Allograft or also known as allogeneous bone grafting is bone graft substitution taken from a donor's body from the same species. Allograft bone substitution has higher incorporation and may cause rejection to the donor's body due to different species. Furthermore, allograft also provides most of the desirable tissue characteristics of autograft. However, it has the risk of transmitting hepatitis and HIV. Others, it also might cause pathogen transmission from donor to host that might lead to infection to occur in the recipient's body after transplantation (Whited et al., 2005).

### **2.3.3 Xenografts Bone Substitution**

Xenograft or also known as xenotransplantation are bone graft substitution taken from a donor's body from different species. Xenotransplantation has an advantage over allograft as it offers virtually unlimited source of organs. However, same as allograft, xenograft also has limitation, where it may cause HIV and hepatitis B virus (Boneva et al., 2001).

Eventhough bone graft substitution treatments are effective in many cases, it still have many difficulties, limitation and disadvantages. Thus, research had been conducted to improve treatment methodology exists (Bandyopadhyay et al., 2006).

Current cell culture methods for tissue-engineered bone grafting materials produce weakly organized sheets of cells. These method cannot withstand the mechanical forces present *in vivo*. However, what is currently needed is bone grafting materials that will permit rapid cell growth and maturation, while providing the initial biomechanical support required for ambulatory function (Bandyopadhyay et al., 2006).

Materials that accomplish this objective will slowly transfer the function to the developing tissue. Lack of such a material prevents clinical use from allowing immediate restoration of functional load bearing. Calcium phosphate based porous biomaterials have considerable potential in these areas and generated significant interest from various research groups in the past two decades (Bandyopadhyay et al., 2006).

## **2.4 Biomaterials**

### **2.4.1 Definition of Biomaterials**

Biomaterials is defined as “an implantable materials that perform its function when in contact with living tissue”. Biomaterials and tissue engineering sciences aim to develop materials that can be used to be implanted in the human body to replace the tissues defects. Biomaterials had already being applied in medical application, for example tooth implants, artificial finger joints and contact lenses. Depending on the tissue to be replaced, different types of materials are being used in body reconstruction functions, so that it can perform their duty for an undefined period of time, that is the rest of the patient’s life (Vallet-regí, 2010).

Biomaterials can be made of three main classes of materials, which are ceramics, metals and polymers. Each class of materials shows some of advantages and drawbacks. Ceramics are the most suitable materials to be implanted in human body as it is a biocompatible materials that can be obtained with biostable, bioactive, or bioresorbable

properties. However, ceramic also has disadvantages in terms of its hardness and fragility. Other than that, metal is popular for their optimum mechanical properties, but it exhibits problems of corrosion and toxicity. Moreover, polymers offer various possibilities that depend on the chemical composition and structure with very few have shown good bioactive properties (Vallet-regí, 2010).

#### **2.4.2 Generation of Biomaterials**

There are three distinct generations in development of biomaterials. These development based on three levels of clinical requirement, which are no harm to tissue (bioinert), tissue-bonding (bioactive) and tissue regeneration (biocompatible). The first generation of biomaterials was expected to meet the most basic and important clinical requirement, that is no harm to the tissue being repaired. Bone plate is an example of implant material used to reconstruct bone that had been fractured. However, due to loose of the implants made from the first generation of biomaterials, further research was carried out to find materials which could improve surface bioactivity that could allow the implants to chemically bound with the host tissue (Hanson et al., 2002). This has lead to the second generation of biomaterials which is bioactive materials that allow direct tissue-bonding. However, low probability of longevity of the first and second generation biomaterials have driven researchers to shift to a new strategy of tissue engineering and regeneration (Hanson et al., 2002). The third generation of biomaterials is bioresorbable materials. These materials act as temporary structure, which able to resorb and allow native tissue to integrate with the implant and replace it after some time (Tan, 2015).

**Table 2.4:** Three generations of biomaterials (Hanson et al. 2002; Tan 2015).

Generation	Clinical Requirements	Examples
First	Bioinert (No harm to tissue)	Alumina (Al <sub>2</sub> O <sub>3</sub> ) Cobalt-chrome (CoCr) alloys
Second	Bioactive (Tissue-bonding)	Hydroxyapatite Calcium phosphate
Third	Bioresorbable (dissolve in body)	Ionic substitution of Hydroxyapatite Magnesium alloys

### 2.4.3 Properties of Biomaterials

Biocompatible is properties of a material in which, the ability of a material to induce no harm to the host body while performing well with host body response in specific application. In a simple word, it is nontoxic to the host body. It is important for biomaterials to be biocompatible in order to ensure that implanted material that being in close contact with living organ or tissue does not cause any harmful effects to host organ or tissue. There are also other properties that biomaterials need to have depending its specific application, for an example, bioinert properties, which means the materials is nonreactive under biological conditions (Eliaz & Metoki, 2017).

**Table 2.5:** Important properties for biomaterials (Hanson et al. 2002; Tan 2015; Eliaz & Metoki 2017).

<b>PROPERTY</b>	<b>FUNCTION</b>
Bioactivity	The ability of a material to react in specific biological or have an effect on living tissues
Biocompatibility	The ability of a material to perform with an appropriate host response in a specific application
Bioactive	Reactive surfaces form chemical bonding with bone, thus minimizing the fibrous capsule formation
Biostability	The ability of a material to maintain its properties <i>in vivo</i>
Osseointegration	Direct anchorage of an implant by the formation of bony tissue around it without growth of fibrous tissue at the bone/implant interface
Osteoconduction	Ability to provide a scaffold for the formation of new bone
Osteoinduction	The process by which osteogenesis is induced. This term means that primitive, undifferentiated and pluripotent cells are somehow stimulated to develop into the bone-forming cell lineage
Resorption	Gradual degradation over time to replace the biomaterial with the natural host tissue
Wettability	The property that indicates a material's ability to attract/repel water molecules

## **2.5 Bioceramics**

### **2.5.1 Introduction to Bioceramics**

Ceramic materials is any inorganic and nonmetallic solids that often are classified according to its applications. For example, ceramic whitewares are ceramic materials that used to produce tableware, sanitary ware and tiles. Technical or advanced ceramic also known as fine ceramics are ceramic materials used to produce semiconductors, structural ceramics and Bioceramics used for biomedical application (Best et al., 2008).

### **2.5.2 Classification of Bioceramics**

Ceramic is an inorganic and non-metallic material. There are three typical classification of bioceramics, this classification is according to the biological reactivity in the body. First classification is bioresorbable ceramics. The implant materials under this category is dissolved and absorbed by the surrounding tissue. Example of materials are silica ( $\text{SiO}_2$ ), calcium monoxide ( $\text{CaO}$ ) and sodium oxide ( $\text{Na}_2\text{O}$ ). Second classification is surface bioactive ceramics. Materials being implant will form a bond across the interface between the tissue and implant to prevent motion between the two surfaces. This to mimic the type of interface that form when tissue undergo self-repair. Example of materials are crystalline hydroxyapatite and calcium phosphate (Best et al., 2008). Third classification is biological near-inert ceramics. The most common response of tissue to an implant from these materials is the formation of non-adherent fibrous capsule. The tissue attempts to reject the implant by creating a barrier around it. Example of materials are alumina ( $\text{Al}_2\text{O}_3$ ) and zirconia ( $\text{ZrO}_2$ ) (Chevalier & Gremillard, 2009).

## 2.6 Calcium Phosphate Bioceramics

### 2.6.1 Calcium phosphate

Calcium phosphate refers to a family of compound minerals that contain calcium ions ( $\text{Ca}^{2+}$ ) and phosphate ions ( $\text{PO}_4^{3-}$ ), the main inorganic phase of bone. Example of the compound minerals are tricalcium phosphate ( $\text{Ca}_3(\text{PO}_4)_2$ ), dicalcium phosphate anhydrous ( $\text{Ca}_2\text{H}_2(\text{PO}_4)_2$ ) and apatite group (Eliaz & Metoki, 2017). Apatite group is a group of phosphate minerals with general formula  $\text{M}_{10}(\text{ZO}_4)_6\text{X}_2$  (Kumar et al., 2012). Apatite name was created in 1786 by Abraham Gottlob Werner, a German geologist which means “to mislead” (Eliaz & Metoki, 2017).

The compound minerals of calcium phosphate are categorized according to their calcium over phosphorous (Ca/P) ratio. Furthermore, the properties of calcium phosphate also vary significantly as a function of porosity, composition and phase. Table 2.6 lists the compound minerals of calcium phosphate with their properties (Dorozhkin & Epple, 2002).

**Table 2.6:** Properties of biologically relevant calcium phosphates (Boanini et al., 2010).

Compound name	Abbreviation	Formula	Ca/P ratio	pH stability	Space group	Density
Monocalcium phosphate monohydrate	MCPM	$\text{Ca}(\text{H}_2\text{PO}_4)_2 \cdot \text{H}_2\text{O}$	0.5	0.0 - 2.0	Triclinic	2.23
Monocalcium phosphate anhydrate	MCPA	$\text{Ca}(\text{H}_2\text{PO}_4)_2$	0.5	[a]	Triclinic	2.58
Dicalcium phosphate dehydrate (brushite)	DCPD	$\text{CaHPO}_4 \cdot 2\text{H}_2\text{O}$	1.0	2.0 - 6.0	Monoclinic	2.32
Dicalcium phosphate anhydrate (monetite)	DCPA	$\text{CaHPO}_4$	1.0	[a]	Triclinic	2.89
Octacalcium phosphate	OCP	$\text{Ca}_8(\text{HPO}_4)_2(\text{PO}_4)_4 \cdot 5\text{H}_2\text{O}$	1.33	5.5 - 7.0	Triclinic	2.61
$\alpha$ -tricalcium phosphate	$\alpha$ -TCP	$\alpha\text{-Ca}_3(\text{PO}_4)_2$	1.5	[b]	Monoclinic	2.86
$\beta$ -tricalcium phosphate	$\beta$ -TCP	$\beta\text{-Ca}_3(\text{PO}_4)_2$	1.5	[b]	Rhombohedral	3.07
Amorphous calcium phosphate	ACP	$\text{Ca}_x(\text{PO}_4)_y \cdot n\text{H}_2\text{O}$	1.2 - 2.2	[e]	Hexagonal	1.75
Calcium-deficient hydroxyapatite	CDHA	$\text{Ca}_{10-x}(\text{HPO}_4)_x(\text{PO}_4)_{6-x}(\text{OH})_{2-x}$ ( $0 < x < 1$ )	1.5 - 1.67	6.5 - 9.5	Hexagonal	1.59
Hydroxyapatite	HA	$\text{Ca}_{10}(\text{PO}_4)_6(\text{OH})_2$	1.67	9.5 - 12	Monoclinic or hexagonal	3.16
Tetracalcium phosphate	TTCP	$\text{Ca}_4(\text{PO}_4)_2\text{O}$	2.0	[b]	Monoclinic	3.05

[a] Stable at temperature above 100°C.

[b] Cannot be precipitated.

[c] Always metastable.

## 2.6.2 Hydroxyapatite

Hydroxyapatite (HA) is a member of apatite group ceramics that has general formula  $M_{10}(ZO_4)_6X_2$  with chemical formula  $Ca_{10}(PO_4)_6(OH)_2$  (Kumar et al., 2012). HA has widely been used in bone reconstructive surgery due its close chemical composition, mimicking to the inorganic phase of the native bone (Kulanthaivel et al., 2015). HA material is well known for its good stability, bioactivity, biocompatibility, non-toxicity and osteoconductivity properties (Baba Ismail et al., 2017).

Hydroxyapatite has a good biocompatibility properties due to its close chemical composition and crystal structure to native bone mineral. Pure HA crystallizes in the monoclinic space group. However, at temperatures above  $250^\circ\text{C}$ , there is a monoclinic to hexagonal phase transition in HA. Some impurities, like partial substitution of hydroxide by fluoride or chloride ions, stabilize the hexagonal structure of HA at ambient temperature. For this reason, the very rare single crystals of natural HA always exhibit a hexagonal space group (S. V. Dorozhkin & Epple, 2002).

**Table 2.7:** Mechanical properties of native bone tissue and hydroxyapatite (Dorozhkin & Epple 2002).

Properties	Bone	Hydroxyapatite
Elasticity modulus (GPa)	0.34 – 13.8	10
Compressive strength (MPa)	150	100

### 2.6.3 Limitation of Hydroxyapatite

Besides, HA also suffers from limited bioactivity, even though it is biocompatible and osteoconductive. This is due to its stability that lead to extremely slow degradation rate in biological fluids, inappropriate degradation rate cause fail to complement *in vivo* bone regeneration (Mickiewicz, 2001). It is known that solubility properties closely related to the chemical reaction with other compound and its biocompatibility of HA with tissue (Kumar et al., 2012).

It also has been emphasized that synthetic HA also has low mechanical strength and poor biological properties as compared to biological bone apatite. Besides, HA also showed poor osteogenic and angiogenic that will lead to low viability of the tissue at the site of bone grafting. It is crucial for the biomaterials designed as bone scaffolds or implants to have both osteogenic and angiogenic properties as bone formation need bone growth factor, as well as blood vessel growth factor for the bone regeneration (Kulanthaivel et al., 2015). Process of bone growth shown in Figure 2.4 below.

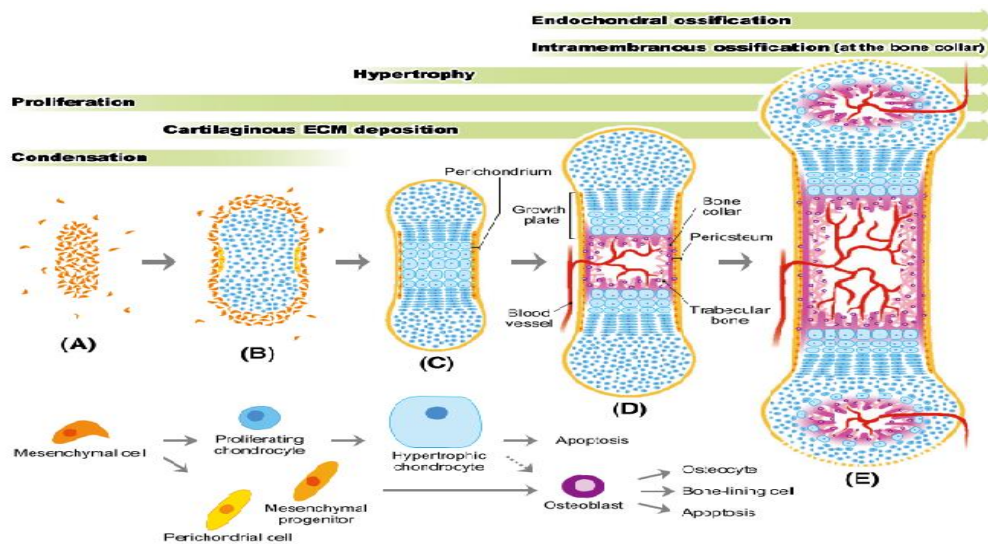


**Figure 2.4:** Long bone development which undergo both osteogenesis and angiogenesis process (Egawa et al. 2014).

It is reported by Kumar et al. (2012) in the literature that the substitution of ions in the HA structure are known to increase the dissolution and degradation rate of the synthetic HA. The substitution could also affect the lattice parameters, surface charge, crystallinity and morphology which can cause changes in thermal stability, mechanical properties and bioactivity of HA.

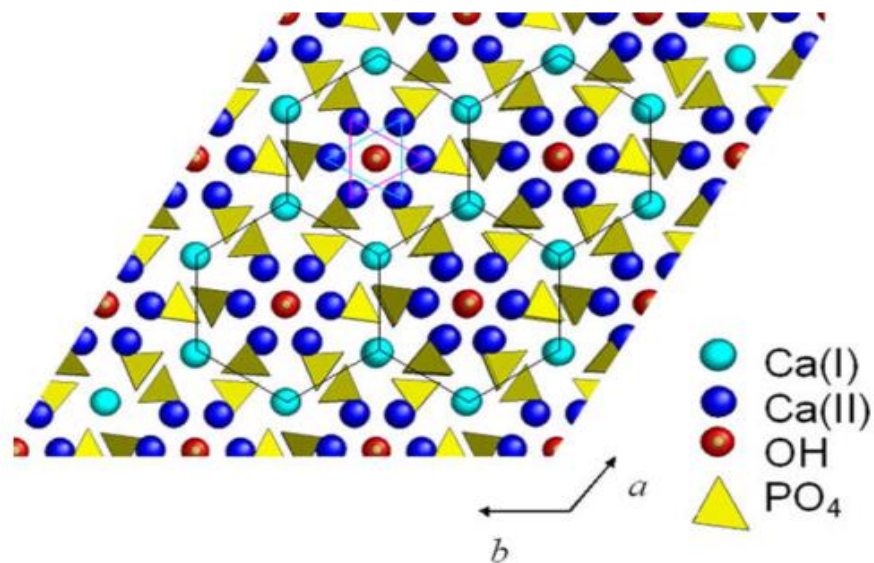


**Figure 2.5:** HA structure from c-axis point of view. Black lines connect Ca(I) columns in hexagonal networks. Cyan and magenta triangles connect staggered Ca(II) atoms lying in the same plane, but at different height with respect to the c-axis (Boanini et al. 2010).

#### 2.6.4 Ionic Substitution in Hydroxyapatite

Hydroxyapatite has an apatite structure that allows for wide compositional variations, which able to accept many different ions in its three sub-lattices. The apatite structure of mineral crystallizes into hexagonal crystal structure that consist of an array of phosphate ions ( $\text{PO}_4^{3-}$ ) tetrahedra held together by calcium ions ( $\text{Ca}^{2+}$ ) and hydroxyl ions ( $\text{OH}^-$ ) ions. This structure allow the substitution of the  $\text{PO}_4^{3-}$  site by  $\text{Ti}^{4+}$ ,  $\text{CO}_3^{2-}$ ,

$\text{SiO}_4^{4-}$  and  $\text{Ca}^{2+}$  site by  $\text{Mg}^{2+}$ ,  $\text{Zn}^{2+}$ ,  $\text{Sr}^{2+}$ , as well as  $\text{OH}^-$  site by  $\text{CO}_3^{2-}$ ,  $\text{F}^-$  and  $\text{Cl}^-$ . There have been many studies in producing synthetic HA containing various substitution in its three sub-lattices, as bone mineral itself is a calcium phosphate apatite containing multiple ionic substitutions and to overcome the limitation of hydroxyapatite (Kulanthaivel et al., 2015).

#### **2.6.4.1 Anionic Substitutions**

Carbonate ions ( $\text{CO}_3^{2-}$ ) is the most abundant ions present in bone, which about 4-8wt%. the substitution of carbonate ions into HA structure can improved the biological activity compared to pure HA, as incorporation of carbonate ions into HA caused a change in crystal morphology, decrease in crystallinity, increase in solubility and increase the local concentration of calcium and phosphate ions that are necessary for new bone formation (Wong & Mohd Noor, 2016).

Substitution of carbonate ( $\text{CO}_3^{2-}$ ) into hydroxyapatite lattice site can produce two type of hydroxyapatite, which are A-type CHA and B-type CHA. A-type CHA will form if carbonate ion substitute into hydroxyl ( $\text{OH}^-$ ) site, while B-type CHA will form if carbonate ion substitute into phosphate ( $\text{PO}_4^{2-}$ ) site (Baba Ismail et al., 2017). A-type CHA usually found in old bone tissue, while B-type CHA usually found in young bone tissue. B-type CHA is preferable due to its commonly found in young tissue, and responsible for the decrease of crystallinity and subsequently increases its solubility (Wong & Mohd Noor, 2016).

Previous study had been conducted by Wong & Mohd Noor (2016) and Baba Ismail & Mohd Noor (2011) found that B-type CHA was successfully synthesized via nanoemulsion method with 4.30 wt% carbonate content. However, there were limitations found during synthesized CHA, as CHA is thermal instability and easy to decompose at

800°C. Sintering at 1100°C by Baba Ismail & Mohd Noor (2011) found that there was transformation from B-type CHA to AB-type CHA and A-type CHA. Furthermore, Baba Ismail & Mohd Noor (2011) also found that sintering at 800°C cause carbonate to decompose. Thus, wet carbonate dioxide (CO<sub>2</sub>) gas was pumped in during cooling stage when temperature reaches 200°C. The wet CO<sub>2</sub> gas not only composite the carbonate loss, but also increase the densification and lead to improvement of mechanical properties. As for Wong & Mohd Noor (2016), it is found that pump in dry CO<sub>2</sub> gas through water compare to direct wet CO<sub>2</sub> gas had overall higher amount of carbonate content.

#### **2.6.4.2 Cationic Substitutions**

Magnesium is the fourth of the highest percentage among minor element in which 0.72% of native bone composition that can acts as a co-factor for many essential enzymes in *in-vivo* conditions. It had been reported that the substitution of magnesium ions (Mg<sup>2+</sup>) in HA structure could stimulate the osteogenesis, which is bone formation process and improve bioactivity compare to pure HA (Laurencin et al., 2011). This substitution could also affect the apatite crystallization and its thermal stability (Kumar et al., 2012).

*In vitro* study conducted by Serre et al. (1998) reported that substitution of 5 wt% magnesium into HA cause a decrease in the proliferation and osteoblast activity likes cells. Furthermore, Landi et al. (2006) reported that substitution of 5.7 wt% magnesium into HA produced no genotoxicity or toxicity. Implanted MgHA granules into New Zealand white rabbits reported that it shows better properties compare with HA as a bone substitute, where resorption was higher compared to stoichiometric HA with slower new bone generation compare with HA. Eventhough bone generation using MgHa slower that HA, it is better conditions due to the composition, nano-dimension and surface characteristics of the MgHA.

There are few reports on the simultaneous substitution of various ions into HA structure. Magnesium ions ( $\text{Mg}^{2+}$ ) substitute resulted in phase decomposition of HA when heated at high temperature. However, simultaneous substitution of magnesium ( $\text{Mg}^{2+}$ ) ions and carbonate ions ( $\text{CO}_3^{2-}$ ) into HA structure made HA thermally stable (Kumar et al., 2012) and better dissolution of synthetic apatites (Kehoe & Eng, 2008).

Besides magnesium ions, cobalt ions has also been investigate recently, where cobalt is a component for vitamin B12, in which vital for angiogenesis, red blood cells production. The substitution of cobalt ions ( $\text{Co}^{2+}$ ) in HA structure have shown positive results particularly in stimulating the angiogenesis, which is the blood vessel formation process and improve the bioactivity, physical, chemical and mechanical properties compare to pure HA (Kulanthaivel et al., 2015). Synthesized of cobalt ions in HA using wet method successfully obtain 0.46 and 3.7 wt9% of cobalt weight in HA reported by Shepherd et al. (2012).

## **2.7 Synthesis of Hydroxyapatite Based Powders**

There are various methods used to prepare HA nanoparticles with precise control over its micro-structure including many types of known chemical synthesis routes. Every type of method for processing conditions can be varied in a wide range, resulting in several sub methods. In present, there are five groups of preparation methods with six subgroups, which are high-temperature processes (with two subgroups), synthesis methods based on biogenic sources and combination procedures (Sadat-shojai et al., 2013). Summary of these classification of methods are shown in Table 2.8.

**Table 2.8:** Type of methods used to synthesize HA nanoparticles (Sadat-shojai et al., 2013).

Method		Processing aspects		Characteristics of powder				
		Number of chemicals	Cost	Morphology	Crystallinity degree	Phase purity	Ca/P ratio	Size
Dry methods	Solid-state method	Few	Low	Diverse	Very high	Usually low	Variable	Usually micron
	Mechanochemical method	Few	Low	Diverse	Very high	Low	Usually non-stoichiometric	Nano
Wet methods	Chemical precipitation	Frequently few	Low	Diverse	Frequently low	Variable	Non-stoichiometric	Usually nano
	Hydrolysis method	Few	Usually high	Diverse	Variable	Usually high	Stoichiometric	Variable
	Sol-gel method	Variable	Variable	Diverse	Variable (usually low)	Variable	Stoichiometric	Nano
	Hydrothermal method	Variable	Usually high	Frequently needle-like	Very high	Usually high	Stoichiometric	Nano or micron
	Emulsion	Many	High	Frequently needle-like (usually needle-like)	Frequently low	Variable	Non-stoichiometric	Nano
	Sonochemical method	Few	Usually low	Diverse (usually needle-like)	Variable	Usually high	Variable	Nano

## 2.8 Apatite Layer Formation

Previous studies reported that osteoconduction process was governed by the formation of apatite layer after the implantation in bone defects. To evaluate the potential of the apatite formation *in vitro*, Kokubo and his colleagues developed a Simulated Body Fluid (SBF) solution that has almost equal concentrations in inorganic ions to those in human blood plasma. Numerous studies have been performed using SBF solution to study the apatite layer formation.

Example of successful apatite formation was done by S. Best et al. (2008). Based on Figure 2.5, it can be seen the apatite layer that form on the surface of the sample after soaking in SBF solution for two weeks. The formation of apatite layer prove that the sample has good bioactivity and indicates that there were interaction between sample and ions from SBF solution. Apatite layer has a beneficial effect on cell adhesion during implantation, in which it has high possibility for bone to regenerate if being implanted in human body (J.Gonzalez Ocampo et al., 2016).

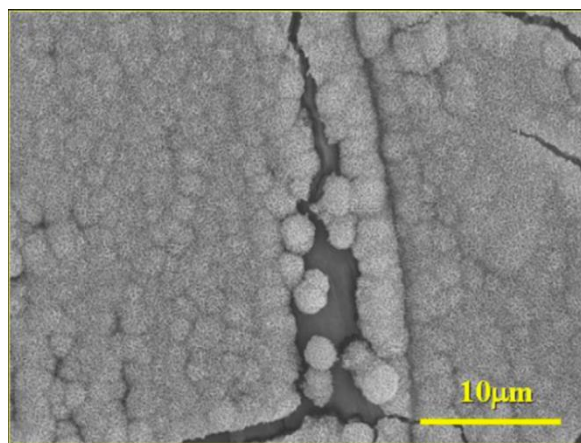


**Figure 2.6:** Apatite layer that formed on the surface of sample after being soaked in SBF solution (S. Best et al., 2008).

## **CHAPTER 3**

### **MATERIALS AND METHODOLOGY**

#### **3.1 Introduction**

In general, there are four stages in this project as being summarized in Figure 1.1 in Chapter 1. Basically, this chapter can be divided into five parts. The first part of this chapter describes the wet chemical method and materials used to synthesis CHA and a range of multi-doped CHA powders via nanoemulsion method, followed by fabrication of dense CHA and dense multi-doped CHA via dry pressing method. The third part of this chapter discussed method to sinter CHA and a range of multi-doped CHA. Next, the fourth part of this chapter discussed materials and method to conduct bioactivity test. Afterwards, the final parts of this chapter discussed about all of characterization method used in this project.

There were eight types of characterization techniques have been used in this research, which were X-Ray Diffraction (XRD), Fourier Transform Infrared Spectroscopy (FTIR), Carbon Hydrogen Nitrogen (CHN) analyzer, X-Ray Fluorescence (XRF), Field Emission Scanning Electron Microscopy/Energy Dispersive X-Ray Spectroscopy (FESEM/EDX), Diametral Tensile Strength (DTS) test, density and porosity test, shrinkage test, and bioactivity test. Characterization is important to choose the optimum composition among four composition of multi-doped CHA powders at the first stage of this project. It is also important to study the mechanical properties of the sintered dense multi-doped CHA. In order to determine the presence of apatite layer, *in-*

*in vitro* bioactivity test was then conducted by immersing the fabricated dense multi-doped CHA in Simulated Body Fluid (SBF).

### 3.2 Synthesis of CHA and Multi-Doped CHA Powders

#### 3.2.1 Materials

The materials that were used to synthesize CHA (as control material) and multi-doped CHA powders are listed in Table 3.1. Calcium nitrate tetrahydrate ( $\text{Ca}(\text{NO}_3)_2 \cdot 4\text{H}_2\text{O}$ ) and di-ammonium hydrogen phosphate ( $(\text{NH}_4)_2\text{HPO}_4$ ) were used as calcium ( $\text{Ca}^{2+}$ ) and phosphate ( $\text{PO}_4^{3-}$ ) precursors. Ammonium bicarbonate ( $(\text{NH}_4)\text{HCO}_3$ ), magnesium nitrate hexahydrate ( $\text{Mg}(\text{NO}_3)_2 \cdot 6\text{H}_2\text{O}$ ) and cobalt nitrate hexahydrate ( $\text{Co}(\text{NO}_3)_2 \cdot 6\text{H}_2\text{O}$ ) were used as sources of carbonate ( $\text{CO}_3^{2-}$ ), magnesium ( $\text{Mg}^{2+}$ ), cobalt ( $\text{Co}^{2+}$ ) precursors. Sodium hydroxide (NaOH) was used to control the pH value at 11.

**Table 3.1:** List of raw materials used in nanoemulsion method and their function.

MATERIALS	CHEMICAL FORMULA	FUNCTIONS	MOLECULAR WEIGHT (g/mol)	SOURCE
Calcium nitrate tetrahydrate	$\text{Ca}(\text{NO}_3)_2 \cdot 4\text{H}_2\text{O}$	Calcium precursor	236.15	Merck
Di-ammonium hydrogen phosphate	$(\text{NH}_4)_2\text{HPO}_4$	Phosphate precursor	132.05	Merck
Ammonium bicarbonate	$(\text{NH}_4)\text{HCO}_3$	Carbonate precursor	79.06	Sigma-Aldrich
Magnesium nitrate hexahydrate	$\text{Mg}(\text{NO}_3)_2 \cdot 6\text{H}_2\text{O}$	Magnesium precursor	256.41	Merck
Cobalt nitrate hexahydrate	$\text{Co}(\text{NO}_3)_2 \cdot 6\text{H}_2\text{O}$	Cobalt precursor	291.03	Sigma-Aldrich
Sodium hydroxide	NaOH	Control the pH value at 11	40.00	Merck
Acetone	$\text{C}_3\text{H}_6\text{O}$	Solvent to make nanoemulsion	58.08	JT. Baker

### 3.2.2 Methodology

Synthesis of carbonated hydroxyapatite (CHA) was done via nanoemulsion method as this method was very favorable to produce nano-sized B-type CHA (Zhou et al., 2008). Furthermore, synthesis of CHA via nanoemulsion was performed by using direct pour technique, instead of dropwise technique. This is because Baba Ismail & Mohd Noor (2011) reported that this technique was more effective compared to dropwise technique as carbonate content obtained from direct pour technique was slightly higher than dropwise technique in their study. As for solvent to dissolve calcium nitrate tetrahydrate, acetone was being used as acetone to dissolve calcium nitrate tetrahydrate without affecting the purity of CHA (Zhou et al., 2008).

Synthesis of CHA and multi-doped CHA was carried out by first added source of carbonate ( $\text{CO}_3^{2-}$ ) precursor,  $(\text{NH}_4)\text{HCO}_3$  solution into source of phosphate ( $\text{PO}_4^{3-}$ ) precursor,  $(\text{NH}_4)_2\text{HPO}_4$  solution via direct pouring technique. Next, the source of calcium ( $\text{Ca}^{2+}$ ) precursor,  $\text{Ca}(\text{NO}_3)_2 \cdot 4\text{H}_2\text{O}$  solution which initially prepared by dissolving in acetone was added into carbonate-phosphate solution to produce gelatinous precipitate with continuous stirring. When  $\text{Ca}(\text{NO}_3)_2 \cdot 4\text{H}_2\text{O}$  solution was added into carbonate-phosphate solution,  $\text{Ca}(\text{NO}_3)_2 \cdot 4\text{H}_2\text{O}$  solution transformed from transparent to milky white solution, as precipitation already took place immediately during the direct pouring process. After the mixing process was done, the pH value of the solution was maintained at pH 11 by dropping NaOH solution. The mixture was then continuously stirred for 30 minutes to ensure complete reaction occurred.

For synthesis of Mg-Co-CHA, both  $\text{Mg}(\text{NO}_3)_2 \cdot 6\text{H}_2\text{O}$  and  $\text{Co}(\text{NO}_3)_2 \cdot 6\text{H}_2\text{O}$  solution were added into the mixture of carbonate-calcium-phosphate solution and continuously stirred for another 30 minutes after each solution were completely added.

Subsequently, the mixture was filtered using Whattman 90 mm filtration set with 542 grade filter paper. Then, the white precipitate was washed with 1 Liter of deionized water for three times to remove any possible residues from the precipitate and dried in oven at 90°C for 24 hours. The dried cake was crushed using an agate mortar and pestle, then 90 µm particles were extracted using a sieve.

Finally, the as-synthesized powders was then characterized physically and chemically using various technique such as XRD, FTIR, CHN, SEM/EDX and XRF to determine the optimum composition of the powders. Figure 3.1 and Figure 3.2 shows flow chart of the process for the synthesis of CHA as control material and multi-doped CHA powders via nanoemulsion technique.

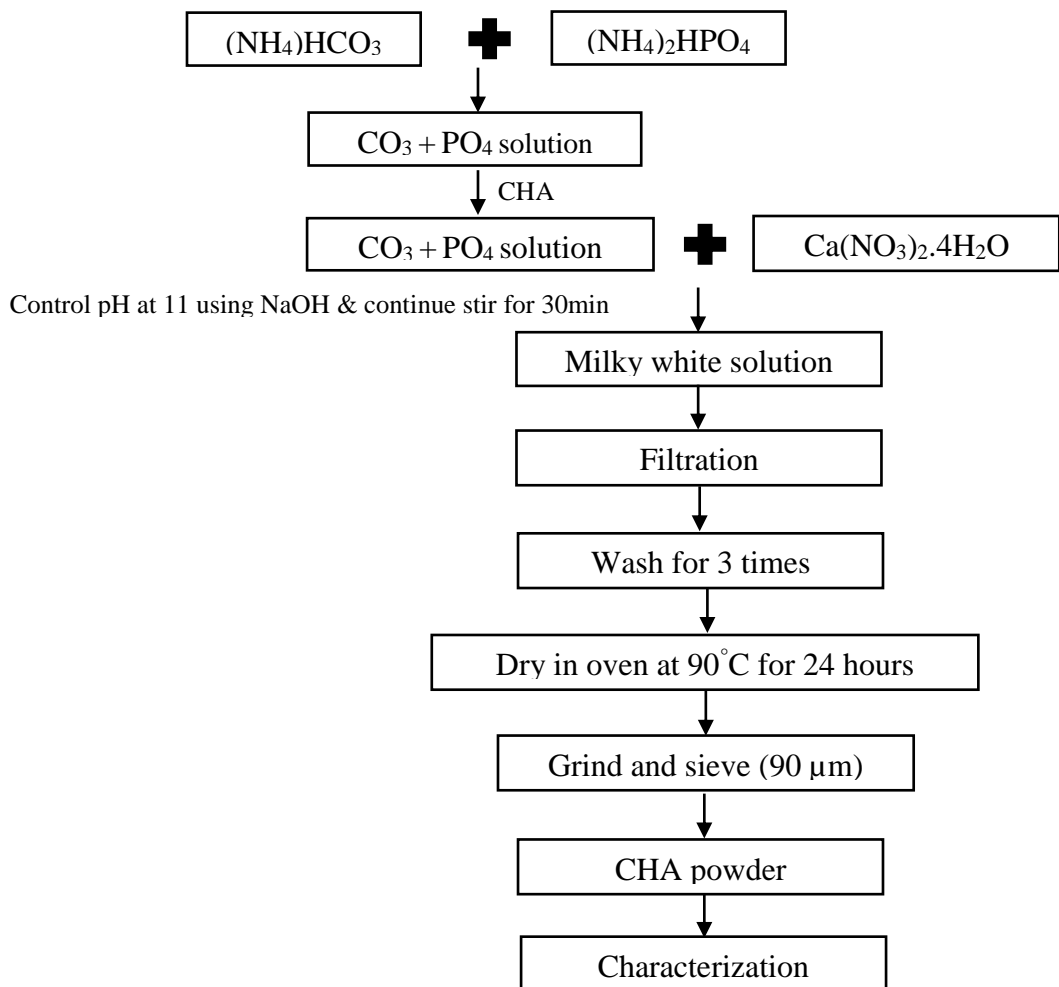


**Figure 3.1:** Process flow to synthesis CHA powders as reference powders.

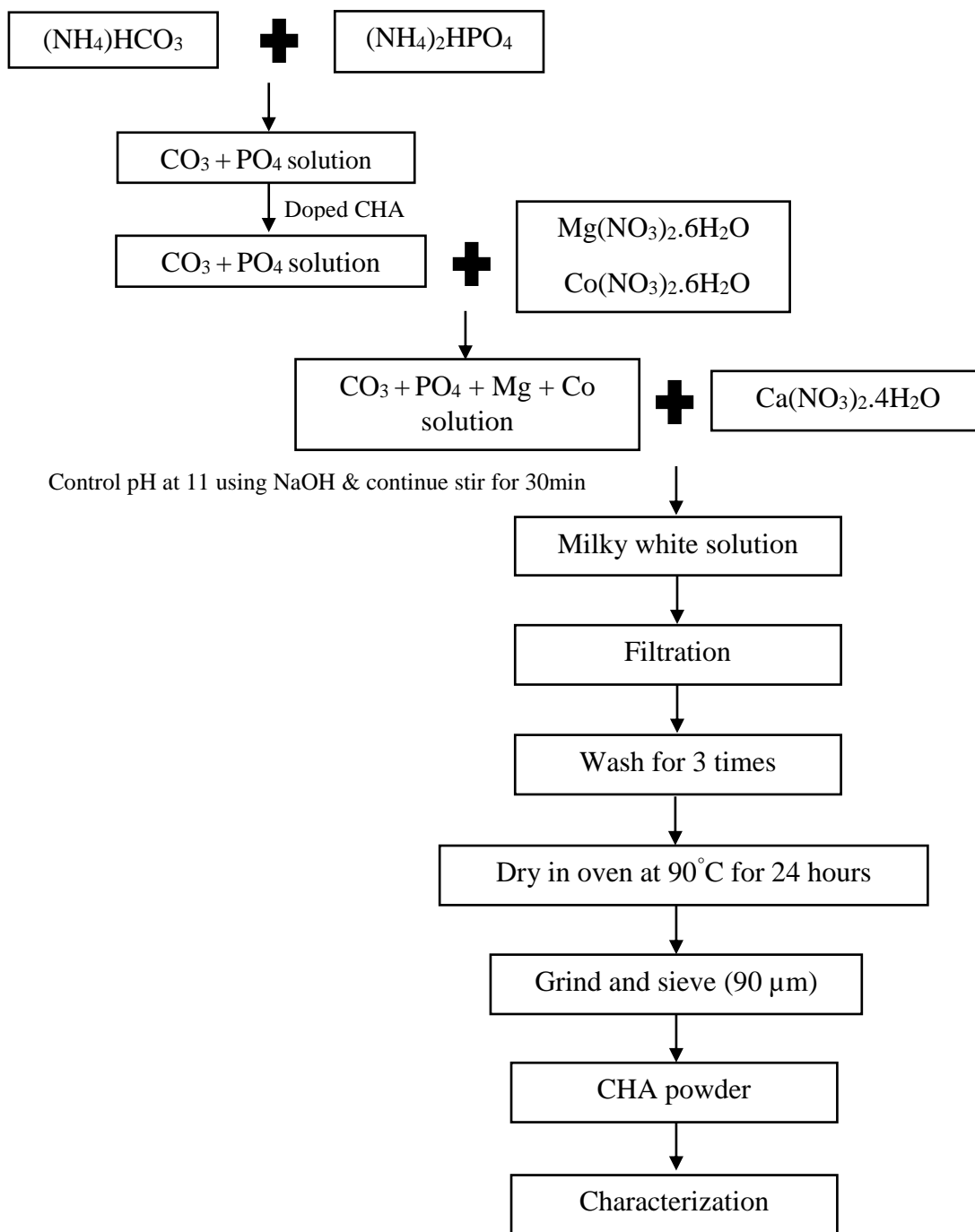


**Figure 3.2:** Process flow to synthesis multi-doped CHA powder.

Based on composition of human bone mineral, it is decided to have four composition to be use in this project. The four composition were named as Mg-Co CHA 1, Mg-Co CHA 2, Mg-Co CHA 3 and Mg-Co CHA 4. Sample Mg-Co CHA 1 was sample with both magnesium and cobalt amount was minimum, 0.60 wt% and  $7.41 \times 10^{-7}$  wt%. This amount was determined based on bone mineral composition as the bone mineral composition given was given in range value, as can observed on Table 3.2. Then, sample Mg-Co CHA 2 was sample with magnesium amount was maximum (0.72 wt%) and cobalt amount was minimum ( $7.41 \times 10^{-7}$  wt%), while sample Mg-Co CHA 3 was sample with both magnesium and cobalt amount was maximum, 0.72 wt% and  $1.23 \times 10^{-6}$  wt%. Finally, Mg-Co CHA 4 was sample with magnesium amount was minimum (0.60 wt%) and cobalt amount was maximum ( $1.23 \times 10^{-6}$  wt%).

**Table 3.2:** Composition of mineral phase in bone (Monika, 2015).

<b>COMPOSITION</b>	<b>CONCENTRATION LEVEL (wt%)</b>
Calcium (Ca)	34.80 – 36.60
Phosphorus (P)	15.20 – 17.10
Carbonates (CO <sub>3</sub> )	4.80 – 7.40
Sodium (Na)	0.90 – 1.00
Magnesium (Mg)	0.60 – 0.72
Chlorine (Cl)	0.10 – 0.13
Fluorine (F)	0.03 – 0.10
Potassium (K)	0.03 – 0.07
Strontium (Sr)	0 – 0.05
Silicon (Si)	0 – 0.05
Zinc (Zn)	0 – $3.9 \times 10^{-3}$
Chromium (Cr)	0 – $3.3 \times 10^{-5}$
Cobalt (Co)	0 – $2.5 \times 10^{-6}$
Manganese (Mn)	0 – $1.7 \times 10^{-5}$

**Table 3.3:** Composition of magnesium and cobalt in each sample.

<b>SAMPLE CODE</b>	<b>COMPOSITION OF MAGNESIUM (wt%)</b>	<b>COMPOSITION OF COBALT (wt%)</b>
Mg-Co CHA 1	0.60 (minimum)	$7.41 \times 10^{-7}$ (minimum)
Mg-Co CHA 2	0.72 (maximum)	$7.41 \times 10^{-7}$ (minimum)
Mg-Co CHA 3	0.72 (maximum)	$1.23 \times 10^{-6}$ (maximum)
Mg-Co CHA 4	0.60 (minimum)	$1.23 \times 10^{-6}$ (maximum)

### **3.3 Fabrication of Dense CHA and Multi-Doped CHA**

Materials used to produce dense multi-doped CHA were chosen among four composition of multi-doped CHA being synthesized. The two optimum composition out of four composition were selected after characterization of powders for all composition had done. Thus, the two optimum composition were Mg-Co CHA 1 and Mg-Co CHA 2. The selection of optimum composition will be discussed more detail in Chapter 4.

Fabrication of dense CHA and multi-doped CHA pellets was done by compacting powders of CHA, Mg-Co CHA 1 and Mg-Co CHA 2 using hydraulic hand press to produce green body of CHA and multi-doped CHA pellets. The powders used to produce each pellets were weighted around 0.5g in order to produce same dimension for each pellets. The powders were then compacted by using a 13 mm diameter die at a pressure of 50 MPa that being held steadily for 120 seconds to ensure that uniform pressure was applied to the samples. Pressure of the hydraulic hand press also was released slowly, as a quick release of the pressure might cause cracking or breaking of the pellet.

### 3.4 Sintering of CHA and Multi-Doped CHA

The green body of dense CHA and multi-doped CHA pellets were then sintered at temperature of 900°C using a Lenton muffle furnace. The heating rate, soaking time and cooling rate for all sintered materials were kept constant. The heating rate was fixed at 9°C/min followed by 2 hours soaking time and cooling rate of 9°C/min as illustrated in Figure 3.3. However, during cooling down, the samples were taken out of furnace at temperature 200°C and immediately placed in a desiccator. In accordance, dry carbon dioxide (CO<sub>2</sub>) gas was pumped into the desiccator for 20 minutes with a rate of 0.5 L/min. Then, the samples were left to be cooled in the desiccator for 24 hours. Carbonate decomposed at temperature above 800°C (Ślósarczyk et al., 2005), thus dry carbon dioxide (CO<sub>2</sub>) gas was used to re-compensate carbon that decomposed during sintering process.

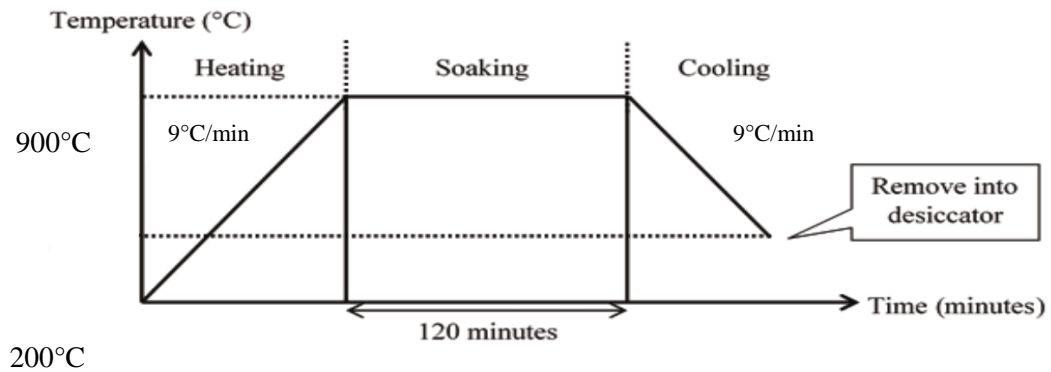


**Figure 3.3:** Sintering profile for sintering process.

### 3.5 Bioactivity Test

#### 3.5.1 Materials

Simulated Body Fluid (SBF) solution was prepared for bioactivity test. There were eight materials used to prepare this solution, which are NaCl, NaHCO<sub>3</sub>, KCl,

$K_2HPO_4 \cdot 3H_2O$ ,  $MgCl_2 \cdot 6H_2O$ , HCl,  $CaCl_2$ ,  $Na_2SO_4$  and  $(CH_2OH)_3CNH_2$  (tris). HCl also was used to control the pH value of the SBF solution at 7.4.

**Table 3.4:** List of raw materials used to prepare 1000 ml SBF solution (Kokubo & Takadama, 2006).

ORDER	MATERIALS	CHEMICAL FORMULA	AMOUNT	FORMULA WEIGHT (g/mol)
1	Sodium chloride	NaCl	8.035g	58.4430
2	Sodium bicarbonate	$NaHCO_3$	0.355g	84.0068
3	Potassium chloride	KCl	0.225g	74.5515
4	Disodium phosphate	$K_2HPO_4 \cdot 3H_2O$	0.231g	228.2220
5	Magnesium chloride hexahydrate	$MgCl_2 \cdot 6H_2O$	0.311g	203.3034
6	Hydrochloric acid	1.0M HCl	39ml	-
7	Calcium chloride	$CaCl_2$	2.65ml	110.9848
8	Sodium sulfate	$Na_2SO_4$	0.072g	142.0428
9	Tris (hydroxymethyl) aminomethane	$(CH_2OH)_3CNH_2$	6.118g	121.1356
10	Hydrochloric acid	1.0M HCl	0–5ml	-

### 3.5.2 Methodology

1000 ml of Simulated Body Fluid (SBF) solution was prepared by preparing 700 ml deionized water and stirring bar in polyethylene beaker. Then, the water was heated to  $36.5 \pm 1.5^\circ C$  in a water bath that being placed on a hot plate.

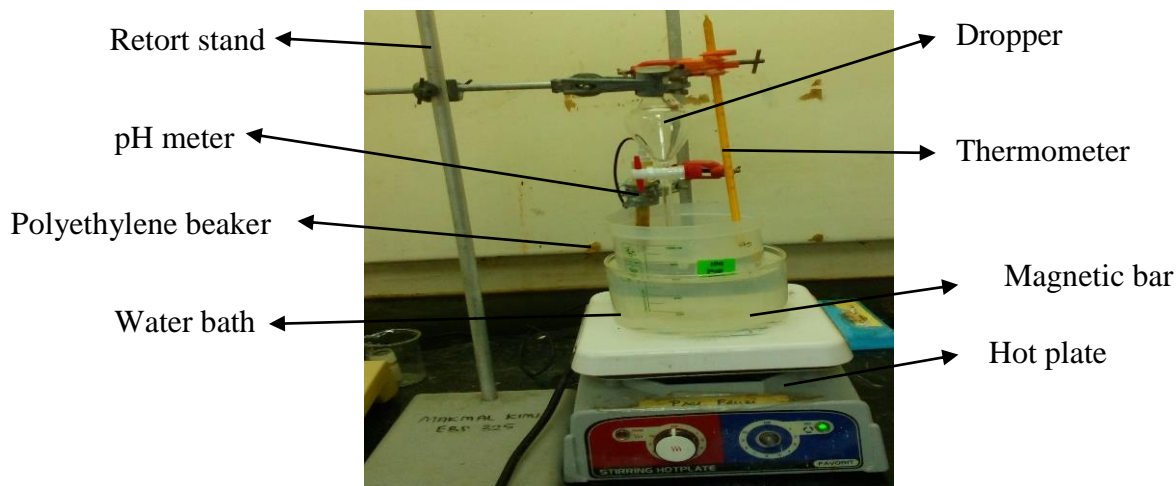


**Figure 3.4:** Setup of apparatus for SBF solution preparation.

Materials were dissolved one by one in order from material one to material eight, ensure that each material completely dissolved before add another material. Furthermore, temperature was kept at  $36.5 \pm 1.5^{\circ}\text{C}$  to stimulate human body temperature. Deionized water was then further added until total solution reached 900 ml. Next, material number nine, which is Tris were added gradually and stoped when pH increase to  $7.45 \pm 0.01$ . This is because increase in pH value lead to precipitation of calcium phosphate (Kokubo & Takadama, 2006). Material number ten, which is hydrochloric acid was dropped by syringe to reduce pH to  $7.42 \pm 0.01$ , but pH should not fall below 7.4. Remaining Tris was continue to dissolve when pH already decreased to  $7.42 \pm 0.01$ . Control pH process was repeated until all Tris already added. As Tris completely added, pH value was adjusted to 7.4, exactly at  $36.5^{\circ}\text{C}$  and deionized water was added to make up 1000 ml. Finally, the solution was transferred to polyethylene bottle when the solution cooled down to  $20^{\circ}\text{C}$  and kept at  $5\text{-}10^{\circ}\text{C}$  in a refrigerator.

The apatite forming ability of the fabricated CHA and multi-doped CHA were investigated by immersing the dense CHA and multi-doped CHA in 20 ml of SBF

solution in polyethylene bottle at  $36.5^{\circ}\text{C} \pm 0.5^{\circ}\text{C}$  for seven days in water bath. SBF solution needed to be change in the day four to ensure there were no precipitation in the solution

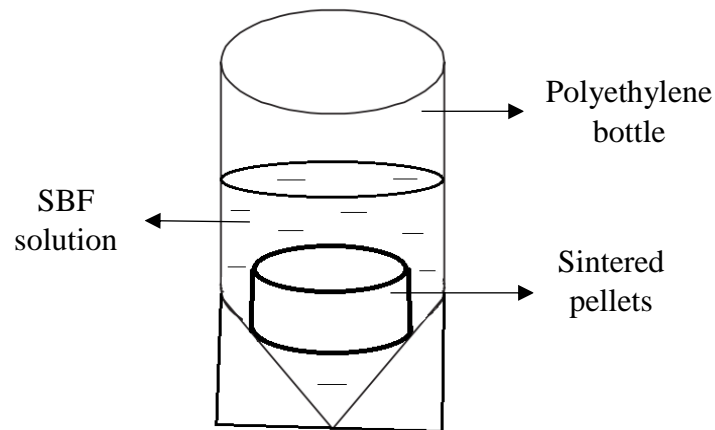


**Figure 3.5:** Schematic diagram of specimen immersed in SBF solution.

### 3.6 Characterization Techniques

Several characterization techniques were used to evaluate the composition of the powders that had been synthesized in terms of its chemical, physical, mechanical and biological properties. Classification of characterization method used based on its function can be seen in Figure 3.6.

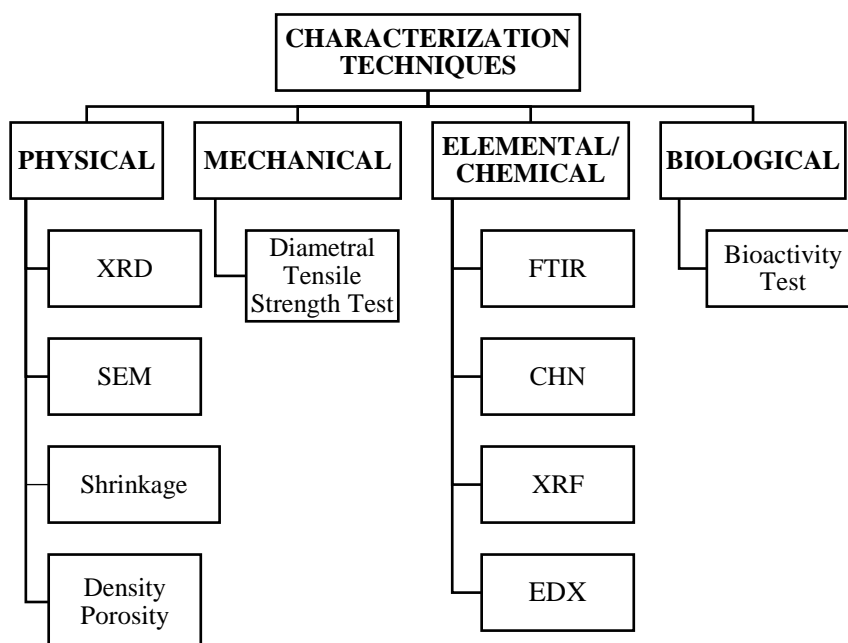


**Figure 3.6:** Classification of characterization techniques used in this study.

### 3.6.1 X-Ray Diffraction

X-Ray Diffraction (XRD) analysis was used to characterize powder that had been synthesized and sintered dense sample in order to determine the crystal structure, lattice parameter and phases formed. The experimental XRD pattern obtained were compared to the standard data of HA pattern using X-Pert HighScore Plus with Joint Committee on Powder Diffraction Standards (JCPDS) files number is 09-0432. The average crystallite size was calculated from XRD data using the Scherrer equation by selecting the most intense peak, from three different samples of the same formulation composition.

XRD machine model used was Buker D8, while spectrum used is Cu  $K_{\alpha}$  radiation with a wavelength,  $\lambda = 1.5406\text{\AA}$ . The scanning range was fixed from  $10^{\circ}$  to  $90^{\circ}$  as to confirm the compound and phase composition. 0.5g of powders were used to make the powder mount for Bragg-Brentano XRD

### **3.6.2 Fourier Transform Infra-Red Spectroscopy**

Fourier Transform Infra-Red (FTIR) spectra was used to determine the mechanism of substitution within the HA structure of the multi-doped CHA powders. FTIR spectra deal with the infrared region of the electromagnetic spectrum to characterize chemical constituents of the sample. Usually, FTIR data were plotted either in transmittance or absorbance spectrum. This indicate at which wavelength the IR was absorbed by the sample which allows the interpretation of the functional group present in the sample.

Sample powder was first ground with potassium bromide (KBr) for sample preparation. Then, the mixed powder was pressed at 28 MPa for two minutes to form a transparent thin pellet. Finally, compacted samples was placed in the FTIR Perkin Elmer Spectrum One machine and characterized using transmittance mode. Wave number range of the FTIR spectra was set up to  $4000\text{ cm}^{-1}$  to  $400\text{ cm}^{-1}$  and scanned for four times.

### **3.6.3 Carbon, Hydrogen, Nitrogen Analyzer**

Carbon, Hydrogen and Nitrogen (CHN) analyzer was used to determine the amount of carbonate presents in the as-synthesized powders. CHN was performed using Perkin Elmer 2400 Series II CHNS/O Elemental Analyzer. CHN analyzer was used to measure carbon concentration in samples, which will be then multiplied by a factor of 5 to estimate the amount of carbonate.

### **3.6.4 X-Ray Fluorescence**

X-Ray Fluorescence (XRF) analysis, an emission spectroscopy was performed using Rigaku RIX 3000, USA to identify element that presence in the sample. In this study, calcium over phosphorous (Ca/P) molar ratio of the as-synthesized powders was

also determined using XRF analysis. Appendix A shows an example calculation of Ca/P molar ratio.

### **3.6.5 Field Emission Scanning Electron Microscopy/Energy Dispersive X-Ray**

Field Emission Scanning Electron Microscopy (FESEM) was used to characterize the surface morphologies of both the powder and dense CHA and multi-doped CHA. FESEM was done to identify the surface morphologies of the powders after synthesized and to determine surface of dense CHA and multi-doped CHA that had been soaked in SBF solution to see the presence of apatite layer.

In order for FESEM to successfully observe the sample, the key requirement for the sample is that it must be electrically conducted. However, samples prepared in this work are non-conductive materials. Thus, a thin conductive coating was required to prevent electrical charging of the sample. Typical heavy metals used to coat the samples are gold, carbon and gold-palladium. For this project, samples were coated with gold before imaging using Zeiss Supra 55VP FESEM.

Energy Dispersive X-Ray (EDX) was used to analyze the elemental of the sample. EDX technique detects x-rays emitted from the sample during bombardment by an electron beam to characterize the elemental composition of the analyzed sample.

### **3.6.6 Linear Shrinkage Measurement**

Linear shrinkage measurement was measured by calculated the change in dimensions of the pellets before and after sintering. The dimensions of the pellets were measured by using digital Vernier caliper and linear shrinkage was calculated by using equation given below in term of diameter and thickness of the pellets.

$$\% D_s = \frac{D_o - D_f}{D_o} \times 100\%$$

$$\% T_s = \frac{T_o - T_f}{T_o} \times 100\%$$

Where,

$D$	= Diameter
$T$	= Thickness
$\%D_s$ and $\%T_s$	= Percent of shrinkage
$D_o$ and $T_o$	= Measurement before sintering
$D_f$ and $T_f$	= Measurement after sintering

The dimensions of the pellets were measured 24 hours after pressing as pellets should not be directly measured and sintered as there would be a spring back effect after pressing process which may cause cracking on the pellets and inaccurate measurement when measured the dimensions. Then, the dimensions of the pellets were measured once again after sintering to calculate the percent of shrinkage.

### **3.6.7 Density and Porosity Measurement**

#### **3.6.7.1 Density of Powders**

Density of powders is a ratio of mass and apparent volume of the powders. The density of powders was calculated using AccuPyc II 1340 Series Pycnometers. This machine measured volume and calculated density automatically using gas (helium gas) displacement technique to measure volume. Density of powders need to be measured in order to calculate relative density of the samples.

#### **3.6.7.2 Apparent Porosity, Bulk Density and Apparent Density of Sintered Pellets**

Apparent porosity and bulk density measurement need dry (D), suspended (S) and saturated (W) weight of the pellets to do the calculation. Dry weight is weight of the

samples before immersed in water, while open pores only filled with air. Suspended weight is a weight of the sample that taken while the sample was submerged in the water. Saturated weight is weight of the samples after immersed in the water, while open pores now filled with water.

The measurement of apparent porosity and bulk density was done by measured the dry weights first. Then, the sample was soaked in deionized water and vacuumed in desiccator for two hours to allow water enter into the pores of the samples. Next, the suspended and saturated weight were measured using Sartorius Balance and Bulk Density Apparatus that followed Archimedes principle. The apparent porosity and bulk density of the samples then calculated using equation given below.

$$\text{Apparent porosity (\%)} = \frac{W-D}{W-S} \times 100\%$$

$$\text{Bulk density, } \rho_{bulk} \text{ (g/cm}^3\text{)} = \frac{D}{W-S}$$

$$\text{Relative density, } \rho_{relative} \text{ (\%)} = \frac{\rho_{bulk}}{\rho_{powder}} \times 100\%$$

Where,

$\rho_{bulk}$	= Bulk density
$\rho_{relative}$	= Relative density
$\rho_{powder}$	= Powder density
$W$	= Wet weight
$D$	= Dry weight
$S$	= Suspended weight

### 3.6.8 Diametral Tensile Strength

Diametral Tensile Strength (DTS) or also known as Brazilian Test involves pressing a sample diametrically, which induce a stress that causes the sample to yield in tension

(Bang et al., 2014). This test was conducted to identify the mechanical strength of the samples.

DTS of compacted sintered samples were tested using INSTRON 3367 universal tensile machine at a strain rate of 0.5 mm/min. In this test, the diameter and thickness of samples were measured before the test begin. Then, the disk shape sample was placed in between two plates and then vertically compressed load was applied until the sample was broke. During loading, the applied force was recorded. Thus, after the testing, the tensile strength was calculated using equation below.

$$\sigma_t = \frac{2P_{max}}{\pi Dt}$$

Where,

$\sigma_t$  = Tensile strength (Nmm<sup>-2</sup>)

$P$  = Maximum applied load (N)

$D$  = Diameter of the sample (mm)

$t$  = Thickness of the sample (mm)

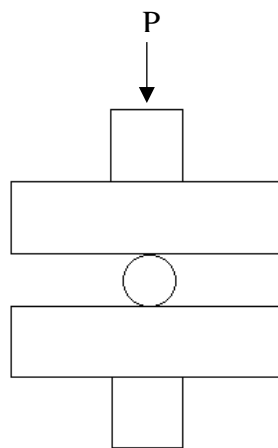


**Figure 3.7:** Schematic diagram of Diametral Tensile Strength (DTS) test.

## **CHAPTER 4**

### **RESULTS AND DISCUSSION**

#### **4.1 Introduction**

In this chapter, the results obtained from the various experiments will be discussed. As discussed earlier in Chapter 3, there were four main stages involved in this study. The first stage involved the synthesis of CHA powder by a nanoemulsion method, which will be used as the control sample and synthesis of a range of multi-doped CHA. This is followed by physico-chemical characterizations in order to determine the optimum composition of multi-doped CHA powders. The results obtained from the analysis will then be presented. In the third stage, the as-synthesized powder with optimum compositions were pelletized and subsequently sintered at 900°C followed by flowing dry carbon dioxide (CO<sub>2</sub>) gas to the samples after cooled down to 200°C as to compensate the carbonate (CO<sub>3</sub>) loss during sintering process. The results and discussion of the dense sintered CHA and multi-doped CHA on physical, chemical, mechanical and biological properties will be presented and compared to relevant work by other researcher at the present time.

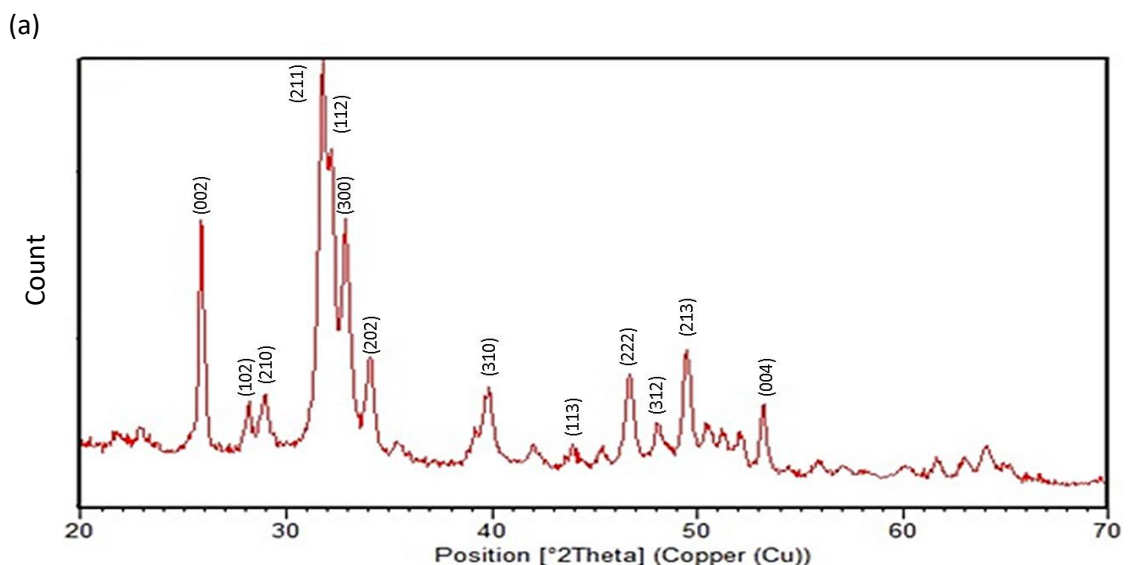
#### **4.2 Synthesis of Carbonated Hydroxyapatite**

In this work, Carbonated Hydroxyapatite (CHA) powders were synthesized by a nanoemulsion method at room temperature. The powders were then characterized physically, chemically and mechanically. XRD, FTIR, CHN, SEM/EDX and XRF analysis were used to find the optimum composition in this stage. XRD and FTIR were performed to identify the phase present and purity of the as-synthesized powders. Then,

CHN was used to estimate the carbonate content in the powders. While, in order to confirm the present of carbonate. XRF was used to calculate the amount of each elements present in the samples. Finally, SEM/EDX analysis were conducted to identify the surface morphology of the as-synthesized powders and also calculate amount of element present in samples at preferred points. In this study, the as-synthesized CHA powders were used as control material in this work.

#### 4.2.1 X-Ray Diffraction

XRD pattern obtained is shown in Figure 4.1. It is observed that the XRD pattern obtained comply with reference XRD pattern of pure HA with the JCPDS file number of 09-0432. The peaks at  $2\theta = 25.86^\circ$  (002),  $2\theta = 28.11^\circ$  (102),  $2\theta = 28.91^\circ$  (210),  $2\theta = 31.75^\circ$  (211),  $2\theta = 32.17^\circ$  (112),  $2\theta = 32.88^\circ$  (300),  $2\theta = 34.04^\circ$  (202),  $2\theta = 39.77^\circ$  (310),  $2\theta = 43.84^\circ$  (113),  $2\theta = 46.66^\circ$  (222),  $2\theta = 48.05^\circ$  (312),  $2\theta = 49.45^\circ$  (213) and  $2\theta = 53.17^\circ$  (004) matches with the major peak of HA (Kumar et al. 2012; Wong & Mohd Noor 2016). It is also confirmed that single phase of CHA was formed, without any presence of secondary phase.



(b)

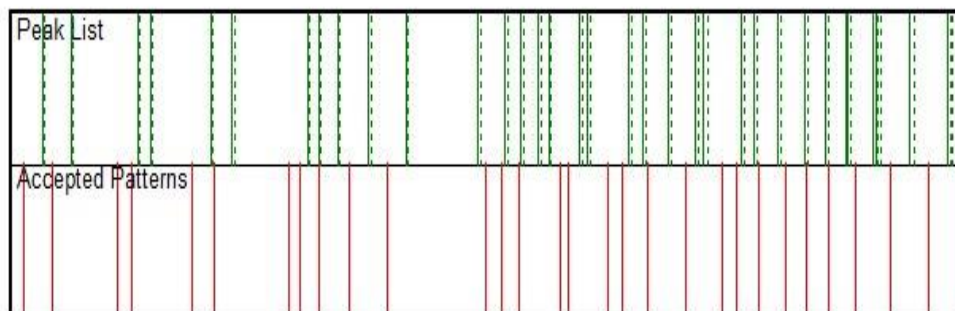


**Figure 4.1:** (a) XRD pattern of CHA based powders without doping that matched with (b) reference pattern of HA.

In this study, the reference database of HA (JCPDS file: 09-0432) was used to determine the type of CHA formed, as the patterns are similar, with only a slight shift of the peak positions. The substitution of carbonate ( $\text{CO}_3$ ) ion in HA structure is less than 10%, that it may not affect the structural pattern of HA. Although there is a reference CHA pattern in the XRD database (JCPDS file:19-0272), it was not being used in this work as the reference do not clearly stated whether it is an A-type CHA or B-type CHA.

The as-synthesized CHA powders were found to be in nano-sized as indicates by the broadness of the peaks obtained. This is also supported by the crystallite size calculated from the X'pert HighScore Plus software. The crystallite size of the as-synthesized CHA powders were found to be about 17.2 nm, smaller compared with previous study by Wong & Noor (2016). Previous study by Wong & Noor (2016) had reported that the size of crystallite size formed was 9.38 nm.

**Table 4.1:** Data obtained by XRD analysis (Batra & Kapoor 2016; Wong & Mohd Noor 2016).

Samples	Phase	Intensity (counts) ( $I_{121}$ )	d (Å) ( $I_{121}$ )	Position ( $^{\circ}2\theta$ ) ( $I_{121}$ )	a=b (Å)	c (Å)	Crystallite Size (nm)
HA REFERENCE (JCPDS 09-0432)	HA	-	-	-	9.4180	6.8840	-
CHA 1	HA	2301.10	2.81628	31.7473	9.4295	6.8857	17.2

It is known that, the carbonate ( $\text{CO}_3^{2-}$ ) ions can possibly substitute either in the hydroxyl ( $\text{OH}^-$ ), phosphate ( $\text{PO}_4^{3-}$ ) or both simultaneously, thus forming A-type CHA, B-type CHA and AB-type CHA (Baba Ismail & Mohd Noor, 2011). Generally, the formation of A-type CHA is indicated by the increase in the *a*-axis ( $>9.418\text{\AA}$ ) and decrease in the *c*-axis ( $<6.884\text{\AA}$ ), while the formation of B-type CHA shows the vice versa effect (Wong & Mohd Noor, 2016). However, the type of CHA obtained in this work could not be confirmed at this stage as both lattice parameters showed the increment. Therefore, FTIR analysis will be presented in the next session to confirm the substitution mode for the as-synthesized CHA powders produced.

#### 4.2.2 Fourier Transform Infra-Red Analysis

Through FTIR analysis, functional group in a molecule can be identified by producing an infrared adsorption spectrum. Therefore, it can be confirmed the type of CHA form either it is an A-type CHA or B-type CHA. Based on Table 4.2, there were list of wave number of carbonate band for A-type CHA and B-type CHA since A-type CHA, carbonate substitute in hydroxyl ( $\text{OH}^-$ ) site, while B-type CHA, carbonate substitute in phosphate ( $\text{PO}_4^{3-}$ ) site.

**Table 4.2:** List of wave number for carbonate band to classify an A-type CHA and B-type CHA (Baba Ismail & Mohd Noor 2011; Wong & Mohd Noor 2016)

A-TYPE CHA ( $\text{cm}^{-1}$ )	B-TYPE CHA ( $\text{cm}^{-1}$ )
877 - 880	870 - 875
1500	1410 - 1430
1540 – 1545	1450 – 1470

Thus, it can be confirmed that CHA nano-powders produced in this work were B-type CHA, since the bands for B-type CHA were detected in FTIR spectrum that can be seen in Figure 4.2. The typical bands for A-type CHA were absent in FTIR spectra produced. Meanwhile, there were also bands that showed the existence of phosphate group, presence of absorbed water and stretching of the hydroxyl group in the FTIR spectra. The typical bands of the HA pattern obtained according to its functional groups is shown in Table 4.3.

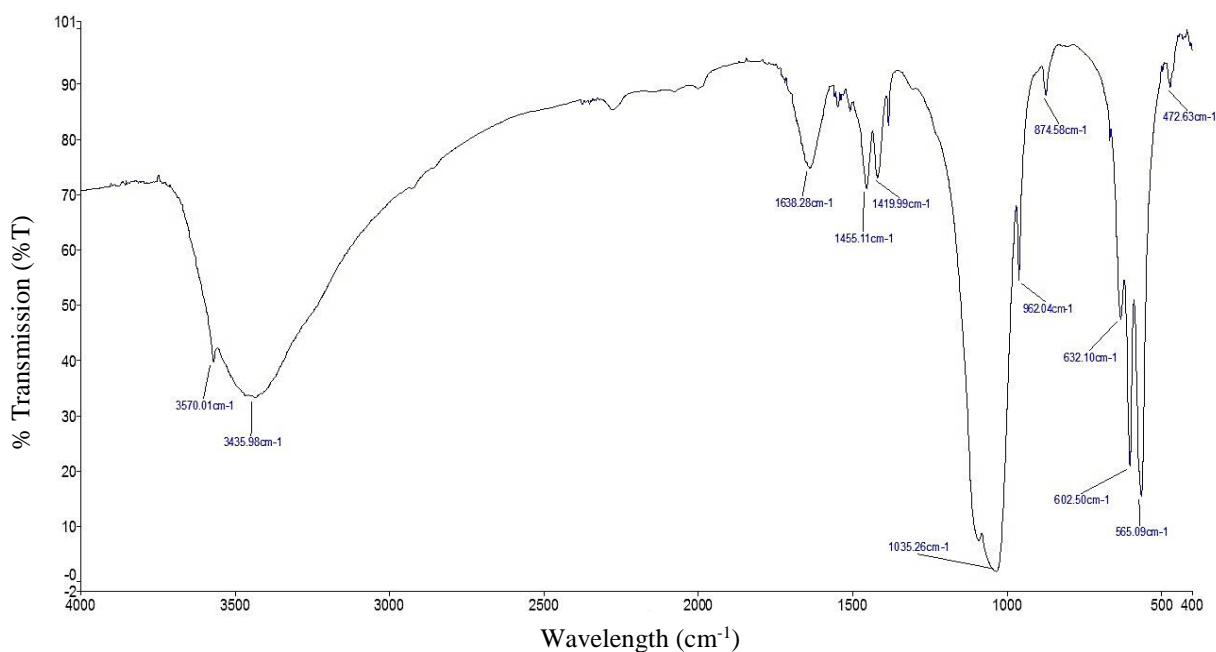


**Figure 4.2:** FTIR spectra of as-synthesized CHA powders.

**Table 4.3:** Typical bands of HA pattern according to its functional groups (Baba Ismail & Mohd Noor 2011; Wong & Mohd Noor 2016).

<b>PHOSPHATE GROUP (PO<sub>4</sub><sup>3-</sup>) (cm<sup>-1</sup>)</b>	<b>ADSORBED WATER (cm<sup>-1</sup>)</b>	<b>OCCLUDED WATER (cm<sup>-1</sup>)</b>
474, 565, 570 - 602, 604, 960, 962, 1032-1072, 1087, 1637 and 3456	1600 - 1700	3200 - 3600

#### 4.2.3 Carbon, Hydrogen, Nitrogen Analysis

To further analyze the CHA powders in quantitative method, CHN elemental analyzer, XRF and EDX were conducted. CHN analysis was conducted to determine the amount of carbonate presence in as-synthesized CHA powders. From CHN analysis, the carbonate (CO<sub>3</sub>) content presence in the as-synthesized CHA powders was found to be 1.75 wt%. This also confirmed that the powder produced was CHA powders.

**Table 4.4:** Amount of carbon and carbonate content in CHA powders.

<b>SAMPLE CODE</b>	<b>WEIGHT PERCENT OF CARBON (wt%)</b>	<b>WEIGHT PERCENT OF CARBONATE (wt%)</b>
CHA	0.35	1.75

#### 4.2.4 X-Ray Fluorescence Analysis

X-Ray Fluorescence (XRF) analysis was conducted to determine the amount of each element, which are phosphorus, calcium, oxygen and calcium to phosphorus ratio in bulk area (whole area of sample). Increasing of calcium to phosphorus ratio also proved that carbonate had been substitute into hydroxyapatite (HA) structure. Furthermore, element

of carbon cannot be detected because carbon had decomposed as XRF required to undergo fusion at 1150°C as its working principle (M. Watanabe, 2015)

**Table 4.5:** XRF results of CHA powder without doping.

	<b>CHA 1 (wt%)</b>
<b>P</b>	12.4061
<b>Ca</b>	23.7836
<b>C</b>	63.8102
<b>Ca/P</b>	<b>1.92</b>

#### **4.2.5 Field Emission Scanning Electron Microscopy/ Energy Dispersive X-Ray**

The surface morphology of as-synthesized CHA powders form were observed using Field Emission Scanning Electron Microscopy (FESEM). Based on the observation, the powders were all agglomerated. Figure 4.3 shows the FESEM image of as-synthesized CHA powders. Due to the agglomeration, it was rather difficult to estimate the actual particle size and shape. In order to do so, TEM analysis will be conducted in the near future. At this state of study, it is assumed that the powders are in nano-size range. This is because when the particles are in nanometer size, it is thus highly charged and tend to agglomerate. In order to get a better dispersed particles, dispersant could be added to prevent powders from aggregating. However, in the present stage of work, this was not emphasized.

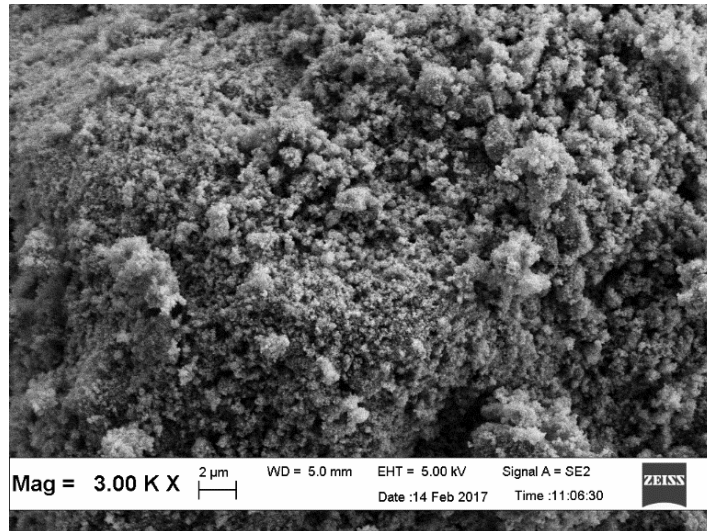


**Figure 4.3:** Surface morphology of as-synthesized CHA powders.

Energy Dispersive X-Ray (EDX) analysis is an elemental analyzer that detect an element in the sample. Results obtained were presented in Table 4.5. Based on Table 4.5, it can be seen the weight percent (wt%) of each element that present in CHA powder, which are carbon, oxygen, phosphorus and calcium. It is shown that, calcium to phosphorus ratio for stoichiometric hydroxyapatite is 1.67 which in agreement with Ramay & Zhang (2003). However, EDX result showed increased in calcium to phosphorus ratio because of the carbonate ( $\text{CO}_3^{2-}$ ) substitution into the phosphate ( $\text{PO}_4^{3-}$ ) group. This confirmed that the CHA powders formed were B-type CHA. The substitution caused a decrease in amount of phosphorus. The decrease in amount of phosphorus (denominator), caused an increase in ratio of calcium to phosphorus.

$$\text{Ratio of calcium to phosphorus} = \frac{\text{Ca (numerator)}}{\text{P (denominator)}}$$

**Table 4.6:** EDX results of CHA powder taken at three preferred points of sample.

	<b>1</b> (wt%)	<b>2</b> (wt%)	<b>3</b> (wt%)	<b>AVERAGE</b> (wt%)
<b>C</b>	7.22	8.67	9.13	8.34
<b>O</b>	27.50	38.49	33.84	33.28
<b>P</b>	23.12	18.59	20.00	20.57
<b>Ca</b>	42.16	34.25	37.03	37.81
<b>Ca/P</b>	1.82	1.84	1.85	1.84

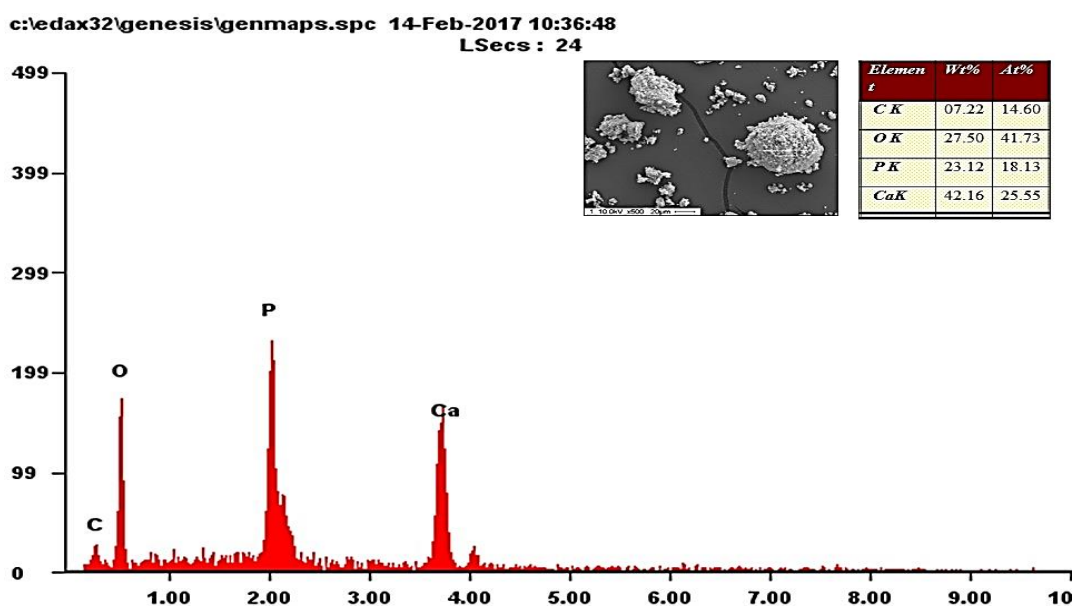


**Figure 4.4:** Actual EDX results of CHA powders taken at preferred points.

However, due to CHA sample was in powder form, detection for the whole area cannot be done, in which it only detect an element at preferred point of sample. Therefore, XRF analysis was conducted to see the amount of each element and calcium to phosphorus ratio in bulk area (whole area of sample). This is because detection at preferred point might have less accuracy in calculating calcium to phosphorus ratio.

### 4.3 Synthesis of Multi-Doped CHA Powders

In this section, the results obtained from the synthesis of multi-doped CHA powders will be presented and discussed. The as-synthesized multi-doped CHA powders were prepared in similar manner as the CHA powders by introducing magnesium ( $Mg^{2+}$ ) ions and cobalt ( $Co^{2+}$ ) ions into the CHA structure. The results obtained were then compared to the CHA powders produced earlier.

#### 4.3.1 X-Ray Diffraction

Figure 4.4 shows the XRD pattern of the as-synthesized multi-doped CHA powders for all compositions. It is observed that all the XRD patterns of the as-synthesized multi-doped CHA perfectly matched with the XRD pattern of CHA powders (produced in this work) and reference XRD pattern of stoichiometric HA with the JCPDS file number of 09-0432. The peaks at  $2\theta = 25.86^\circ$  (002),  $2\theta = 28.11^\circ$  (102),  $2\theta = 28.91^\circ$  (210),  $2\theta = 31.75^\circ$  (211),  $2\theta = 32.17^\circ$  (112),  $2\theta = 32.88^\circ$  (300),  $2\theta = 34.04^\circ$  (202),  $2\theta = 39.77^\circ$  (310),  $2\theta = 43.84^\circ$  (113),  $2\theta = 46.66^\circ$  (222),  $2\theta = 48.05^\circ$  (312),  $2\theta = 49.45^\circ$  (213) and  $2\theta = 53.17^\circ$  (004) based on the CHA powders comply with the major peak of HA (Wong & Mohd Noor, 2016). As for multi-doped CHA, all of four compositions showed the presence of the same peaks CHA powders without any additional peaks. The main peaks of HA,  $31.75^\circ$ ,  $32.17^\circ$  and  $32.88^\circ$  which corresponds to the planes (211), (112) and (300) were present in all compositions (Kulanthaivel et al. 2015). This indicates that doping materials, which are magnesium ( $Mg^{2+}$ ) ions and cobalt ( $Co^{2+}$ ) ions substituted were in small amounts. Therefore, no obvious changes can be seen on the XRD pattern.

However, the peaks were shift slightly to the right, as can be seen in the XRD pattern of multi-doped CHA from Figure 4.5. Based on Table 4.6, it was proven that the peaks were shift slightly to the right as the position of the main peak, which corresponds to the

planes (211) increasing for all compositions compare to the position of based CHA, which position at 31.7473. This might indicates the substitution of magnesium ( $Mg^{2+}$ ) ions and cobalt ( $Co^{2+}$ ) ions in the structure. It is reported that doping of bivalent metal ions has an influence on the crystal structure of HA (Lima et al., 2013). This generally happens because of the size mismatch of the doped ions with calcium ( $Ca^{2+}$ ) ions. Replacement of high ionic radius of  $Ca^{2+}$  (0.099 nm) by low ionic radii of  $Mg^{2+}$  (0.071 nm) and  $Co^{2+}$  (0.070 nm) caused contraction and change the d-spacing as can be seen of Table 4.6 (Kulanthavel et al., 2015). The contraction of the crystal lattice lead to decrease in the crystallinity. Thus, this explained the reason broadening of the peaks for doped CHA, as compared with based CHA. There were also decrease in the intensity of the peaks as can be seen on Table 4.6, where the intensity of the main peaks decreasing for all compositions compared to base CHA. Decrease in intensity were also generally associated with the decreasing in the crystallinity and crystal size of HA.

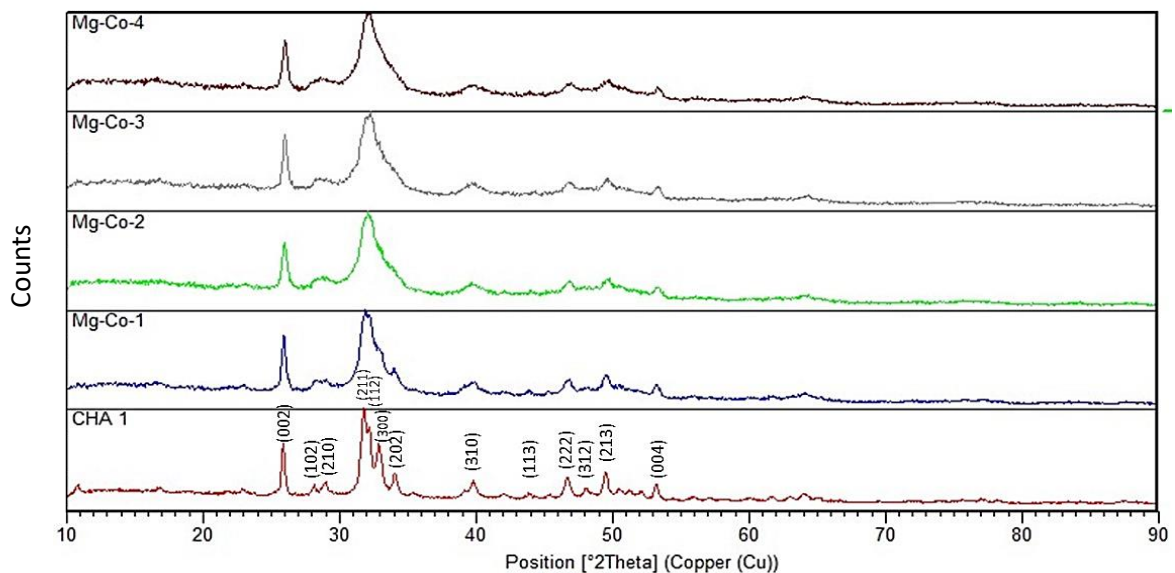


**Figure 4.5:** XRD pattern of as-synthesized multi-doped CHA powders.

**Table 4.7:** XRD data of as-synthesized multi-doped CHA powders.

Samples	Phase	Intensity (counts) (I <sub>121</sub> )	d (Å) (I <sub>121</sub> )	Position (°2θ) (I <sub>121</sub> )	a=b (Å)	c (Å)	Crystallite Size (nm)
CHA 1	HA	2301.10	2.81628	31.7473	9.42945	6.88574	17.2
Mg-Co 1	HA	1550.35	2.81248	31.7913	9.44041	6.89304	9.5
Mg-Co 2	HA	1157.21	2.80856	31.8369	9.44821	6.89650	7.0
Mg-Co 3	HA	1114.14	2.80664	31.8591	9.46119	6.90363	7.0
Mg-Co 4	HA	1090.42	2.80501	31.8781	9.44961	6.90492	7.0

### 4.3.2 Fourier Transform Infra-Red Spectroscopy

FTIR spectra in Figure 4.5 showed the presence of the characteristics bands for all composition of doped CHA that corresponds to CHA powders. It is confirmed that multi-doped CHA formed were still B-type CHA as wave number bands for B-type, which are 874 cm<sup>-1</sup>, 1420 cm<sup>-1</sup> and 1455 cm<sup>-1</sup> were presents in all compositions of the multi-doped CHA as also observed previously by Baba Ismail et al. (2017). However, 1455 cm<sup>-1</sup> band did not present in composition 3 and 4 of multi-doped CHA. Meanwhile, there were also the typical bands at HA detected such as the phosphate group, absorbed water and stretching of the hydroxyl group in the FTIR spectra.

Doping of magnesium and cobalt into CHA structure did not affect band position of the as-synthesized multi-doped CHA powders. However, there were variations in the intensity of bands between compositions 1(Mg-Co CHA 1) to compositions 4(Mg-Co CHA 4) of doped CHA, as being reported bivalent ion in the ionic lattice of HA only affects the bands intensity (Kulanthaivel et al., 2015). It also may because of a very small amount addition of doping that lead to no affect to band position and no occurrence of a new characteristic band.

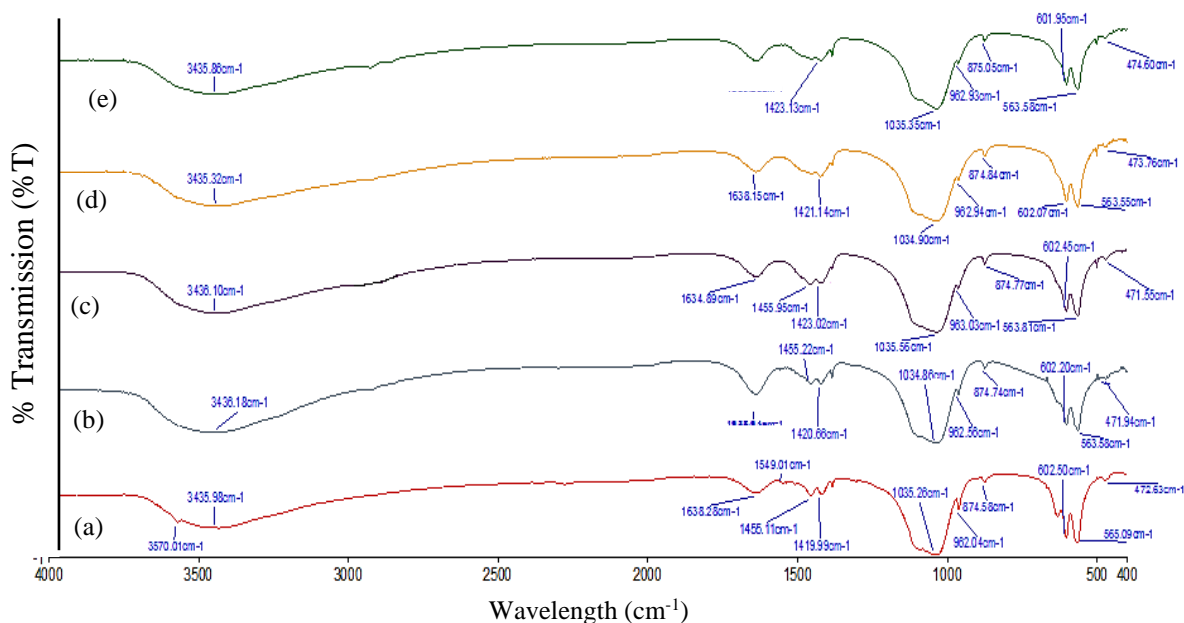


**Figure 4.6:** FTIR spectra of the as-synthesized multi-doped CHA powders compared with CHA powders. (a) CHA, (b) Mg-Co CHA 1, (c) Mg-Co CHA 2, (d) Mg-Co CHA 3 and (e) Mg-Co CHA 4.

### 4.3.3 Carbon, Hydrogen, Nitrogen Analyzer

Each sample produced were confirmed have the presence of carbonate through CHN analysis. From CHN analysis, the carbonate ( $\text{CO}_3$ ) content presence in the as-synthesized CHA and multi-doped CHA powders were calculated by multiplied carbon content data obtained from CHN analysis result with factor of five. The weight percent of carbon and carbonate content in each sample were presented in Table 4.7. Referred to Table 4.7, Mg-Co CHA 2 has the highest amount of carbonate, while the lowest is CHA. Highest amount of carbonate needed as carbon will decomposed at  $800^\circ\text{C}$  during sintering. Therefore, highest amount of carbonate needed.

**Table 4.8:** Amount of carbon and carbonate content in CHA and multi-doped CHA.

<b>SAMPLE CODE</b>	<b>WEIGHT PERCENT OF CARBON (wt%)</b>	<b>WEIGHT PERCENT OF CARBONATE (wt%)</b>
CHA	0.35	1.75
Mg-Co CHA 1	0.56	2.80
Mg-Co CHA 2	0.90	4.50
Mg-Co CHA 3	0.73	3.65
Mg-Co CHA 4	0.57	2.85

#### **4.3.4 X-Ray Fluorescence**

XRF analysis was conducted to determine the amount of each element present in the as-synthesized multi-doped CHA powders, which are phosphorus, calcium, oxygen, magnesium, cobalt and calcium to phosphorus ratio in bulk area (whole area of sample). It is observed that calcium over phosphorous (Ca/P) ratio of the as-synthesized multi-doped CHA powders were higher than calcium over phosphorous (Ca/P) ratio of HA, which is 1.67. Increasing of calcium to phosphorus (Ca/P) ratio also proved that carbonate and the doping elements, magnesium and cobalt ions had been substituted into hydroxyapatite (HA) structure. This supported the FTIR analysis. However, the amount of cobalt could not be detected in composition 3 (Mg-Co CHA 3) and composition 4 (Mg-Co CHA 4). This might be due to the very small amount of cobalt introduced during synthesis, thus, XRF cannot detect their presence in the structure as the smallest amount that XRF can detect was 0.0001 wt%.

**Table 4.9:** XRF results of as-synthesized multi-doped CHA.

<b>Elements Detected</b>	<b>Mg-Co 1 (wt%)</b>	<b>Mg-Co 2 (wt%)</b>	<b>Mg-Co 3 (wt%)</b>	<b>Mg-Co 4 (wt%)</b>
<b>Mg</b>	0.2194	0.2705	0.2414	0.2292
<b>P</b>	11.0832	11.0525	11.1453	11.1425
<b>Ca</b>	20.9509	20.9910	21.6058	21.7217
<b>Co</b>	0.0072	0.0080	-	-
<b>O</b>	67.7402	67.6780	67.0074	66.9066
<b>Ca/P</b>	1.8903	1.8992	1.9386	1.9494

#### **4.3.5 Field Emission Scanning Electron Microscopy/ Energy Dispersive X-Ray**

Field Emission Scanning Electron Microscopy (FESEM) was conducted to observe the surface morphology of the multi-doped CHAs powders. Based on the observation, it can be seen that agglomeration of the powder formed, where it is the same as can be seen in the CHA powders. Figure 4.7 shows the morphology of the as-synthesized multi-doped CHA powders. However, individual particles cannot be detected through FESEM analysis.

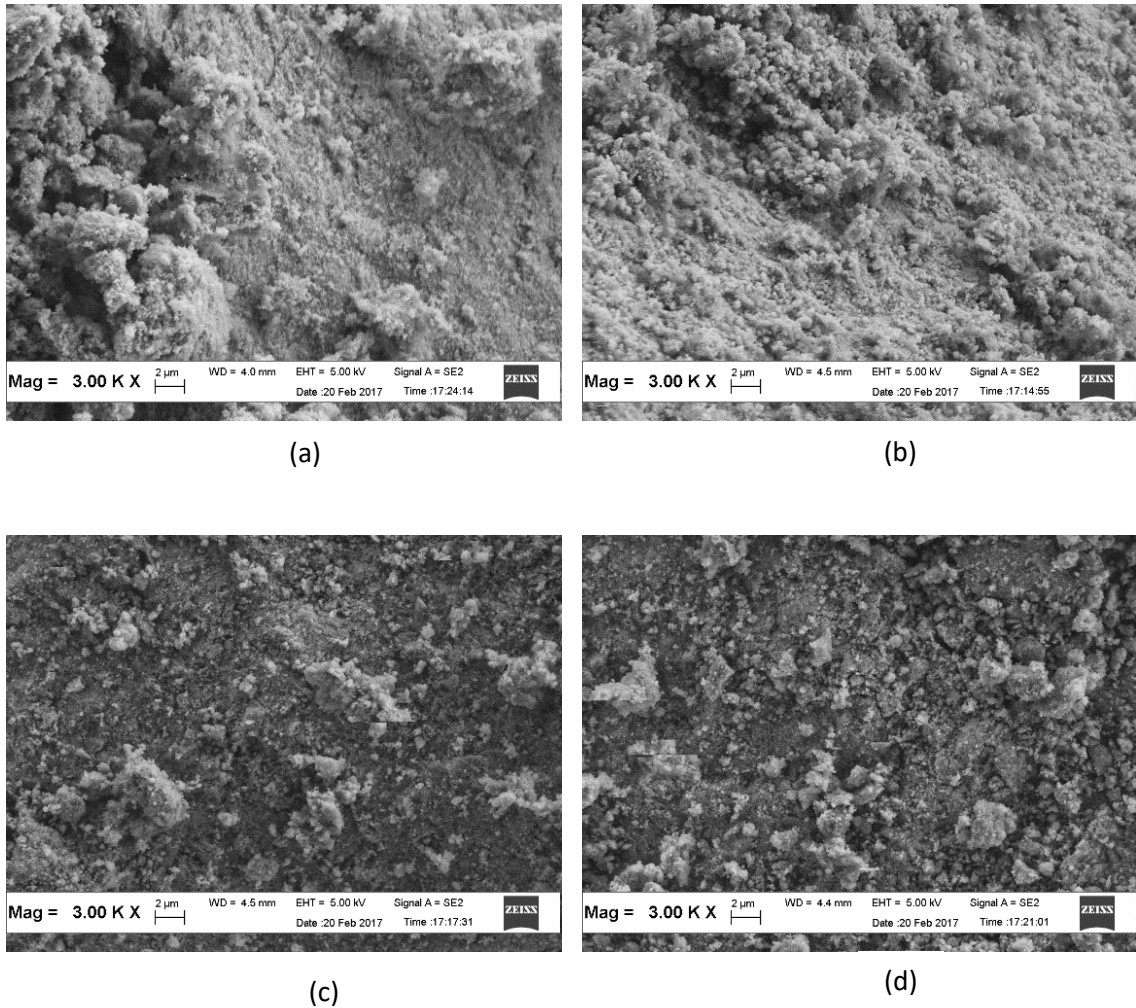


**Figure 4.7:** Surface morphology of the as-synthesized multi-doped CHA powders. (a) Mg-Co1, (b) Mg-Co2, (c) Mg-Co3 and (d) Mg-Co4.

Energy Dispersive X-Ray (EDX) analysis is an elemental analyzer that can be used to detect an element at preferred point of sample if sample in powder form. Results obtained for EDX analysis are presented in Table 4.9. Based on Table 4.9 (a) to (d), it can be seen the weight percent (wt%) of each element present in multi-doped CHA powders, which are carbon, oxygen, phosphorus, calcium, magnesium and cobalt. Based on Table 2.6, calcium to phosphorus (Ca/P) ratio for hydroxyapatite is 1.67. However, EDX result show an increased in (Ca/P) ratio. This indicates that the doping of magnesium and cobalt ions into CHA structure had causes decrease in the amount of phosphorus because there

were substitution occur. Decrease in amount of phosphorus (denominator), cause an increase in ratio of (Ca/P). Thus, the increased in (Ca/P) ratio also can be said that magnesium and cobalt ions were successful doped into CHA structure.

**Table 4.10:** EDX results for the as-synthesized multi-doped CHA, (a)Mg-Co CHA 1, (b) Mg-Co CHA 2, (c) Mg-Co CHA 3 and (d) Mg-Co CHA 4.

(a)

<b>Elements</b>	<b>1</b> (wt%)	<b>2</b> (wt%)	<b>3</b> (wt%)	<b>AVERAGE</b> (wt%)
<b>C</b>	4.73	4.85	8.48	6.02
<b>O</b>	27.14	24.14	32.17	27.82
<b>P</b>	21.24	21.72	19.18	20.71
<b>Ca</b>	44.50	47.26	36.39	42.72
<b>Co</b>	1.52	1.34	2.87	1.91
<b>Mg</b>	0.87	0.70	0.90	0.82
<b>Ca/P</b>	2.10	2.18	1.90	2.06

(b)

<b>Elements</b>	<b>1</b> (wt%)	<b>2</b> (wt%)	<b>3</b> (wt%)	<b>AVERAGE</b> (wt%)
<b>C</b>	7.74	9.00	9.53	8.76
<b>O</b>	37.76	29.91	31.97	33.21
<b>P</b>	17.84	20.01	19.30	19.05
<b>Ca</b>	32.36	37.86	35.88	35.37
<b>Co</b>	3.22	2.00	1.89	2.37
<b>Mg</b>	1.08	1.22	1.44	1.25
<b>Ca/P</b>	1.81	1.89	1.86	1.86

(c)

<b>Elements</b>	<b>1</b> (wt%)	<b>2</b> (wt%)	<b>3</b> (wt%)	<b>AVERAGE</b> (wt%)
<b>C</b>	12.34	8.41	13.36	11.37
<b>O</b>	30.20	25.95	28.39	28.18
<b>P</b>	18.57	20.26	18.39	19.07
<b>Ca</b>	35.93	43.57	36.72	38.74
<b>Co</b>	1.99	0.97	2.20	1.72
<b>Mg</b>	0.95	0.83	0.95	0.91
<b>Ca/P</b>	1.93	2.15	2.00	2.03

(d)

<b>Elements</b>	<b>1</b> (wt%)	<b>2</b> (wt%)	<b>3</b> (wt%)	<b>AVERAGE</b> (wt%)
<b>C</b>	8.14	11.26	7.43	8.94
<b>O</b>	37.14	23.61	36.52	32.42
<b>P</b>	17.55	19.79	18.91	18.75
<b>Ca</b>	33.86	43.49	34.88	37.41
<b>Co</b>	2.39	1.02	1.47	1.63
<b>Mg</b>	0.92	0.83	0.79	0.85
<b>Ca/P</b>	1.93	2.20	1.84	2.00

However, as being mentioned before, detection for the whole area cannot be done in EDX analysis as doped CHA sample was in powder form, in which it only detect an element at preferred point of sample. Therefore, XRF analysis was conducted to see the amount of each element and calcium to phosphorus ratio in bulk area (whole area of sample). This is because detection at preferred point might have less accuracy in calculating calcium to phosphorus ratio.

#### 4.4 Fabrication of Dense Multi-Doped CHA

Dense CHA doped with magnesium and cobalt were fabricate into pellet form and sintered at 900°C. The sintered pellets were then being characterized in terms of their elemental, physical and mechanical properties. Basically, XRD and FTIR analysis were conducted to analyze the phase present and purity of the pellets form and carbonate content after sintering process, as it is known that carbonate decompose at temperature above 800°C (Ślósarczyk et al., 2005). While, linear shrinkage measurement, density and porosity measurement and DTS were conducted to identify the physical and mechanical properties of the sintered dense multi-doped CHA.

##### 4.4.1 X-Ray Diffractions

Figure 4.8 presents the XRD pattern of pure CHA sintered at 900°C. Analysis of the data obtain showed that it is perfectly matched with the XRD pattern of pure HA with the JCPDS file number of 09-0432. The main peaks of reference HA which are at  $2\theta = 25.95^\circ$  (002),  $2\theta = 28.20^\circ$  (102),  $2\theta = 28.91^\circ$  (210),  $2\theta = 31.86^\circ$  (211),  $2\theta = 32.17^\circ$  (112),  $2\theta = 32.99^\circ$  (300),  $2\theta = 34.14^\circ$  (202),  $2\theta = 39.89^\circ$  (310),  $2\theta = 43.94^\circ$  (113),  $2\theta = 46.77^\circ$  (222),  $2\theta = 48.16^\circ$  (312),  $2\theta = 49.55^\circ$  (213) and  $2\theta = 53.26^\circ$  (004) matches with the peak of pure CHA (Wong & Mohd Noor 2016)(Kumar et al. 2012; Wong & Mohd Noor 2016). It also confirmed that single phase of CHA was formed, without presence of secondary phase, concluded that sintering process was done without changing the composition of CHA.

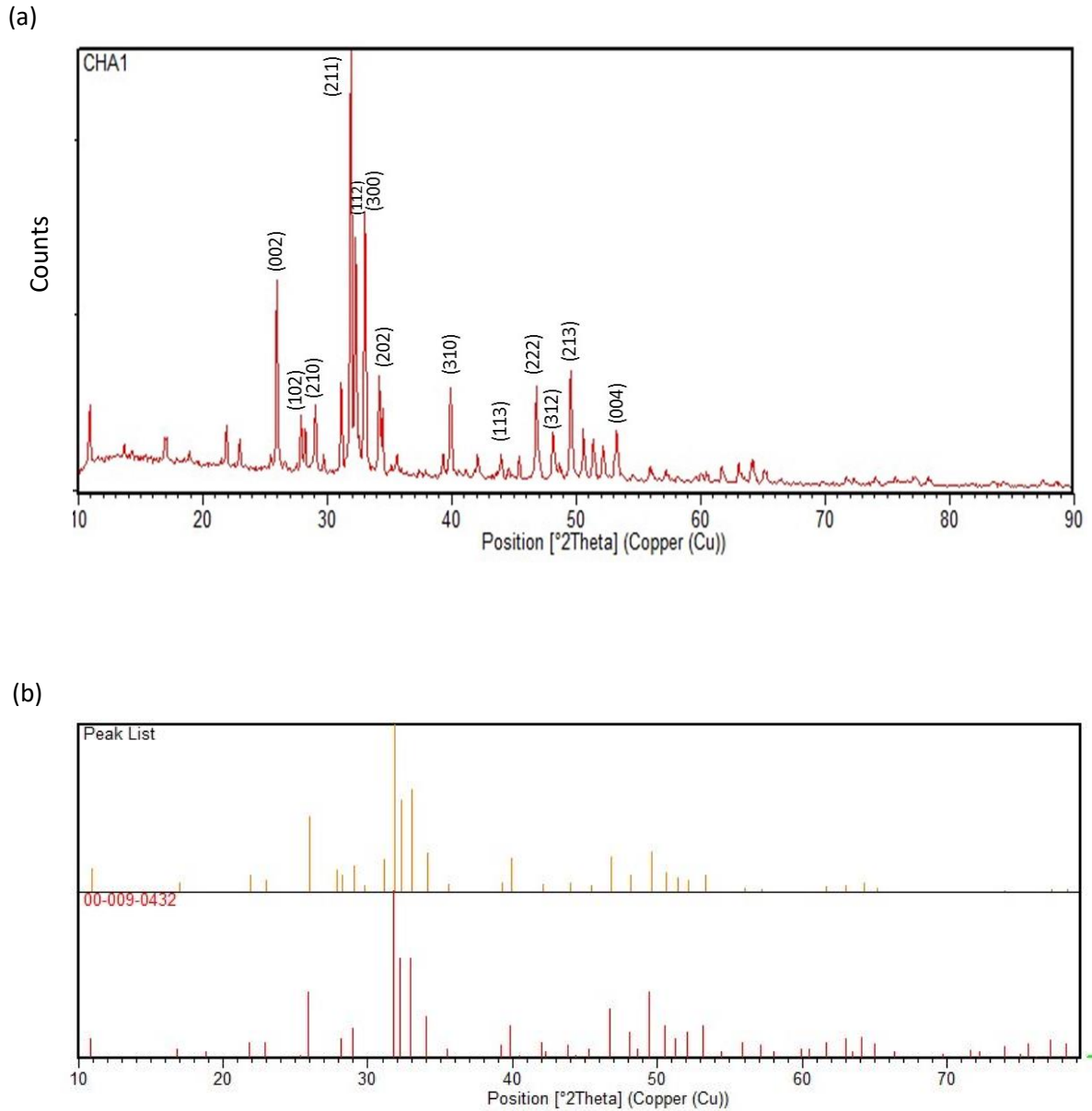


**Figure 4.8:** (a) XRD pattern of sintered pure CHA which comply with (b) HA reference pattern.

Sintered CHA also showed a sharper and narrower XRD patterns, which can be translated as a crystalline structure was formed when the sample undergo sintering process. The Figure 4.9 compares the XRD patterns of pure CHA before and after sintering process, where as-synthesized CHA powders before sintering showed a broad

peak as compared to the dense CHA after sintering. This trend was also observed by Zilm et al. (2015).

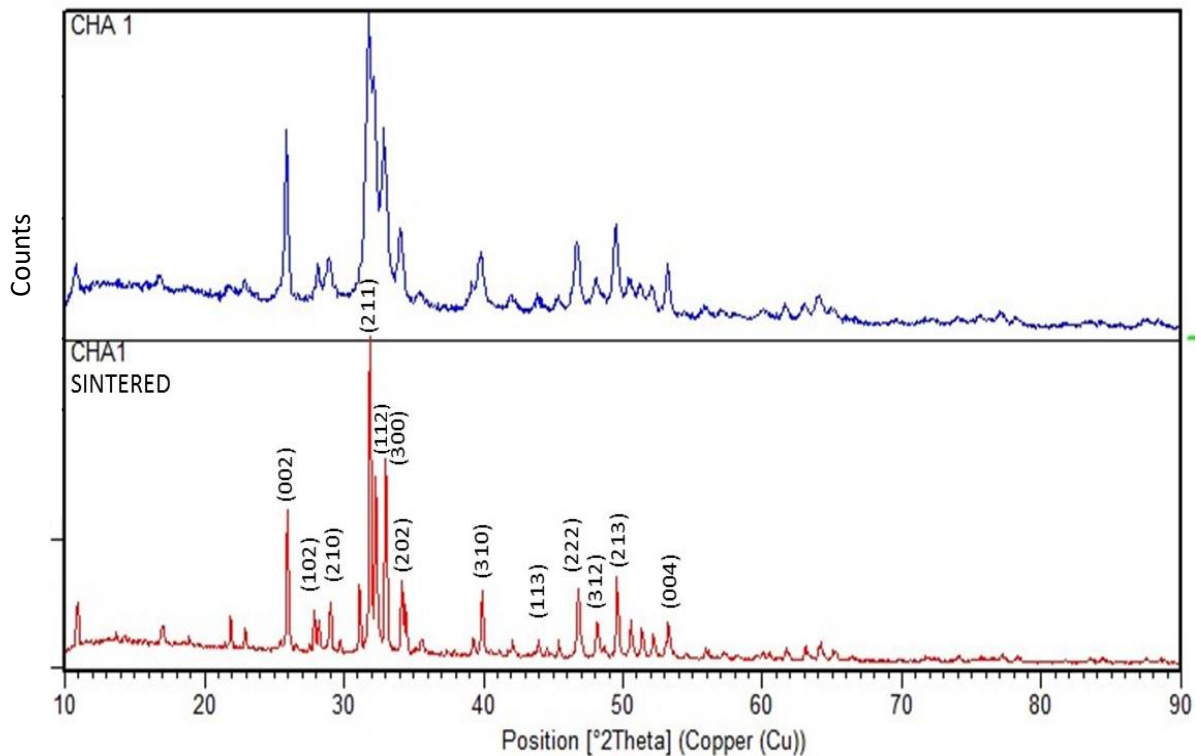


**Figure 4.9:** Comparison of XRD pattern between pure CHA before sintering and after sintering.

Other than the XRD patterns become sharper, there were also changes in lattice parameters and crystallite size. This changes can be observed from XRD data based on Table 4.10. There was slightly contraction on a-axis, while a slightly expansion on c-axis after sintering. Due to sintering process, the crystallite size constantly increased as it able to growth with decreasing in term of micro-strain. The increase of the crystallite size and decrease of the micro-strain of CHA directly resulted in the increased stability, respectively (Guo et al., 2003). The lattice parameters changed due to substitution of carbonate ions into HA structure.

**Table 4.11:** XRD data of sintered dense CHA.

Samples	Phase	Intensity (counts) ( $I_{121}$ )	d (Å) ( $I_{121}$ )	Position ( $^{\circ}2\theta$ ) ( $I_{121}$ )	a=b (Å)	c (Å)	Crystallite Size (nm)
HA REFERENCE (JCPDS 09-0432)	HA	-	-	-	9.4180	6.8840	-
CHA before sintering	HA	2301.10	2.81628	31.7473	9.4295	6.8857	17.2
CHA after sintering	HA	4398.73	2.80688	31.8564	9.4241	6.8858	57.0

Figure 4.10 shows the XRD pattern of optimum composition of multi-doped CHA, Mg-Co CHA 1 and Mg-Co CHA 2 that had been compacted, sintered at 900°C and supply carbon dioxide gas after cooling at 200°C. It is observed that all the XRD patterns of the as-synthesized multi-doped CHA perfectly matched with the XRD pattern of CHA powders (produced in this work) and reference XRD pattern of stoichiometric HA with the JCPDS file number of 09-0432. The peaks at  $2\theta = 25.95^{\circ}$  (002),  $2\theta = 28.20^{\circ}$  (102),  $2\theta = 28.91^{\circ}$  (210),  $2\theta = 31.86^{\circ}$  (211),  $2\theta = 32.17^{\circ}$  (112),  $2\theta = 32.99^{\circ}$  (300),  $2\theta = 34.14^{\circ}$  (202),  $2\theta = 39.89^{\circ}$  (310),  $2\theta = 43.94^{\circ}$  (113),  $2\theta = 46.77^{\circ}$  (222),  $2\theta = 48.16^{\circ}$  (312),  $2\theta = 49.55^{\circ}$  (213) and  $2\theta = 53.26^{\circ}$  (004) based on the sintered CHA based were comply with the major peak of HA (Wong & Mohd Noor, 2016). As for Mg-Co CHA 1 (min-min) and Mg-Co CHA 2 (max-min), both of the compositions showed the presence of the same peaks as CHA based without any additional peaks. The main peaks of HA,  $31.75^{\circ}$ ,  $32.17^{\circ}$  and  $32.88^{\circ}$  which corresponds to the planes (211), (112) and (300) were present in all compositions (Kulanthaivel et al., 2015). This indicates that doping materials, which are magnesium ( $Mg^{2+}$ ) ions and cobalt ( $Co^{2+}$ ) ions substituted were in small amounts. Therefore, no obvious changes can be seen on the XRD pattern.

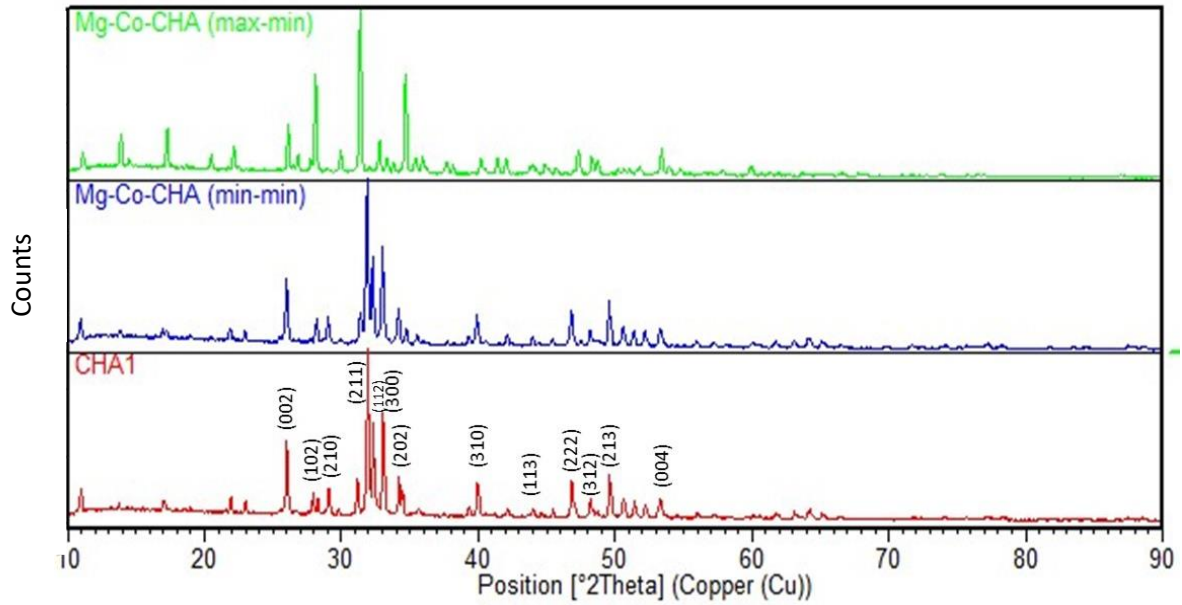


**Figure 4.10:** XRD pattern of sintered multi-doped CHA pellets.

However, the peaks were shift slightly to the left, as can be seen in the XRD pattern of multi-doped CHA from Figure 4.10. Data represented in Table 4.11 proved that the peaks were shift slightly to the left as the position of the main peak, which corresponds to the planes (211) decreasing compare to the main peak position of based CHA, which position at 31.8564.

**Table 4.12:** XRD data of sintered dense multi-doped CHA.

Samples	Phase	Intensity (counts) (I <sub>121</sub> )	d (Å) (I <sub>121</sub> )	Position (°2θ) (I <sub>121</sub> )	a=b (Å)	c (Å)	Crystallite Size (nm)
HA REFERENCE (JCPDS 09-0432)	HA	-	-	-	9.4180	6.8840	-
CHA 1	HA	4398.73	2.80688	31.8564	9.4241	6.8858	57.0
Mg-Co CHA 1	HA	3619.44	2.81146	31.8032	9.4258	6.8832	48.3
Mg-Co CHA 2	HA	4315.11	2.85998	31.2497	9.24862	6.97684	43.0

#### 4.4.2 Fourier Transform Infra-Red Spectroscopy

Figure 4.11 shows that dense CHA samples sintered at 900 °C and cooled down in dry carbon dioxide (CO<sub>2</sub>) atmosphere was remained as pure B-type CHA. This was confirmed by the carbonate peaks bands at 870-875cm<sup>-1</sup> was present in the FTIR spectrum of CHA based. While, the characteristic bands of A-type CHA at about 877-800 cm<sup>-1</sup>, 1500 cm<sup>-1</sup> and 1540-1545cm<sup>-1</sup> were not detected at all in the FTIR spectrum (Baba Ismail & Mohd Noor 2011; Baba Ismail et al. 2017). Furthermore, the characteristic bands of phosphorous (PO<sub>4</sub><sup>3-</sup>) at about 474, 565, 570 - 602, 604, 960, 962, 1032-1072, 1036, 1087, 1637 and 3456, absorbed water at about 1600 - 1700cm<sup>-1</sup> and occluded water at about 3200 - 3600cm<sup>-1</sup> were detected in the FTIR spectra.

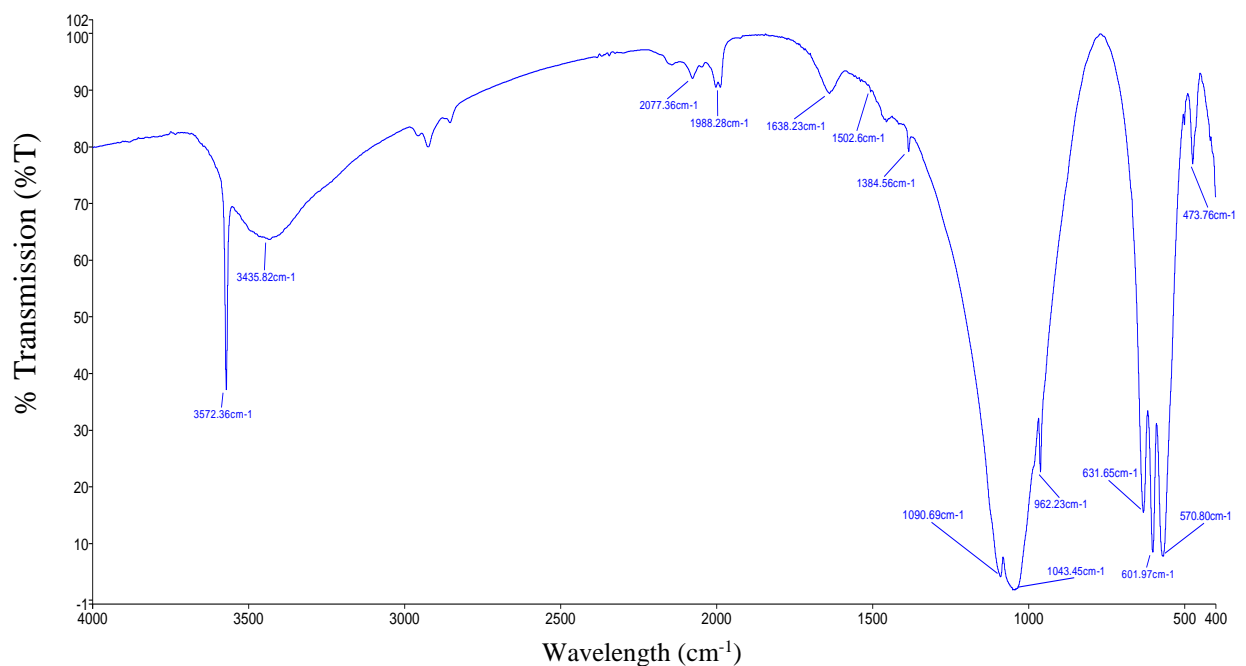


**Figure 4.11:** FTIR spectra of sintered CHA based without doping.

The characteristic bands for B-type CHA also were detected in Mg-Co CHA 1 and Mg-Co CHA 2. Characteristic bands of phosphorous, absorbed water and occluded water

also detected in the FTIR spectra. It was also found that the FTIR bands for all compositions were narrow after sintering compared to FTIR spectra before sintering process. This is due to crystallization that happen during sintering process.

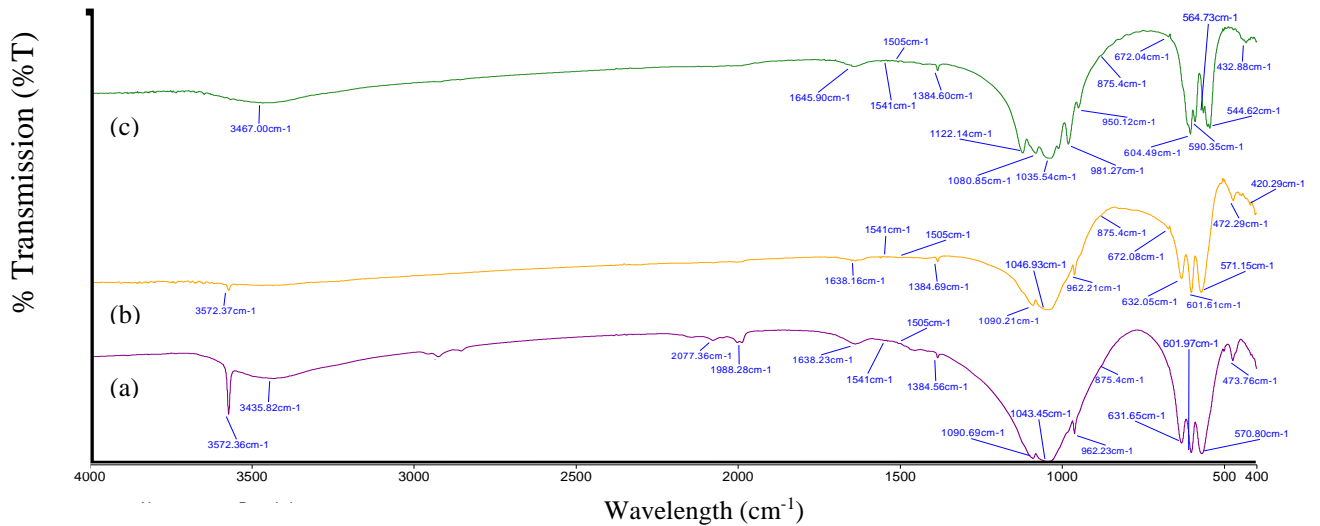


**Figure 4.12:** FTIR spectra of sintered multi-doped CHA compared with CHA based. (a) CHA based, (b) Mg-Co CHA 1 and (c) Mg-Co CHA 2.

#### 4.4.3 Linear Shrinkage Measurement

Shrinkage measurement was conducted to identify the shrinkage behavior of CHA and multi-doped CHA that being sintered at 900°C, followed by cooling in dry carbon dioxide (CO<sub>2</sub>) gas. As the green body of dense CHA and multi-doped CHA undergo sintering process, it decreases in volume and reduction of dimensions as ceramic grains being compacted and bond to each other (Ring & Ring, 1996).

Table 4.12 provides the data of average diameter and thickness measured for CHA and percentage of shrinkage for both in diameter and thickness. Reading of diameter and thickness were taken three times per sample, then average reading for both diameter and

thickness were presented. There were three pellets used to measure the percentage of shrinkage and the data show uniform trend for both shrinkage in diameter and thickness.

**Table 4.13:** Average diameter, average thickness and percent of shrinkage for (a) Diameter and (b) Thickness of CHA.

(a)

Diameter (D)			
	Diameter Initial ( $D_o$ )	Diameter Final ( $D_f$ )	Percent Shrinkage (% $D_s$ )
Pellet 1	13.09	11.91	9.01
Pellet 2	13.11	11.87	9.48
Pellet 3	13.08	11.87	9.25
Average			9.25

(b)

Thickness (T)			
	Thickness Initial ( $T_o$ )	Thickness Final ( $T_f$ )	Percent Shrinkage (% $T_s$ )
Pellet 1	2.56	2.31	9.88
Pellet 2	2.58	2.29	11.00
Pellet 3	2.30	2.09	9.12
Average			10.00

Data of average diameter, thickness measured and percentage of shrinkage for both in diameter and thickness for Mg-Co CHA 1 and Mg-Co CHA 2 were presented in Table 4.13 and Table 4.14. Similarly with CHA, reading of diameter and thickness were taken three times per sample, then average reading for both diameter and thickness were presented. There were also three pellets used to measure the percentage of shrinkage and the data for multi-doped CHA also show uniform trend for both shrinkage in diameter and thickness.

**Table 4.14:** Average diameter and percent of diameter shrinkage for (a) Mg-Co CHA 1 and (b) Mg-Co CHA 2.

(a)

	Diameter (D)		
	Diameter Initial (D <sub>o</sub> )	Diameter Final (D <sub>f</sub> )	Percent Shrinkage (%D <sub>s</sub> )
Pellet 1	13.06	11.19	14.34
Pellet 2	13.06	11.21	14.14
Pellet 3	13.06	11.15	14.62
Average			14.24

(b)

	Diameter (D)		
	Diameter Initial (D <sub>o</sub> )	Diameter Final (D <sub>f</sub> )	Percent Shrinkage (%D <sub>s</sub> )
Pellet 1	13.08	11.05	15.57
Pellet 2	13.05	10.98	15.86
Pellet 3	13.04	11.00	15.60
Average			15.68

**Table 4.15:** Average thickness and percent of thickness shrinkage for (a) Mg-Co CHA 1 and (b) Mg-Co CHA 2.

(a)

	Thickness (T)		
	Thickness Initial (T <sub>o</sub> )	Thickness Final (T <sub>f</sub> )	Percent Shrinkage (%T <sub>s</sub> )
Pellet 1	2.90	2.51	13.56
Pellet 2	2.73	2.39	12.45
Pellet 3	2.72	2.38	12.48
Average			12.83

(b)

	Thickness (T)		
	Thickness Initial (T <sub>o</sub> )	Thickness Final (T <sub>f</sub> )	Percent Shrinkage (%T <sub>s</sub> )
Pellet 1	2.68	2.25	15.92
Pellet 2	2.45	2.06	16.05
Pellet 3	2.71	2.32	14.16
Average			15.38

Shrinkage percentage of CHA, Mg-Co CHA 1 and Mg-Co CHA 2 data presented showed that Mg-Co CHA 2 has the highest shrinkage of diameter and thickness, followed by Mg-Co CHA 1 and CHA. Thus, all of the samples had been densified as shrinkage occur. Due to low percent of shrinkage, there is no significant formation of crack found on the samples.

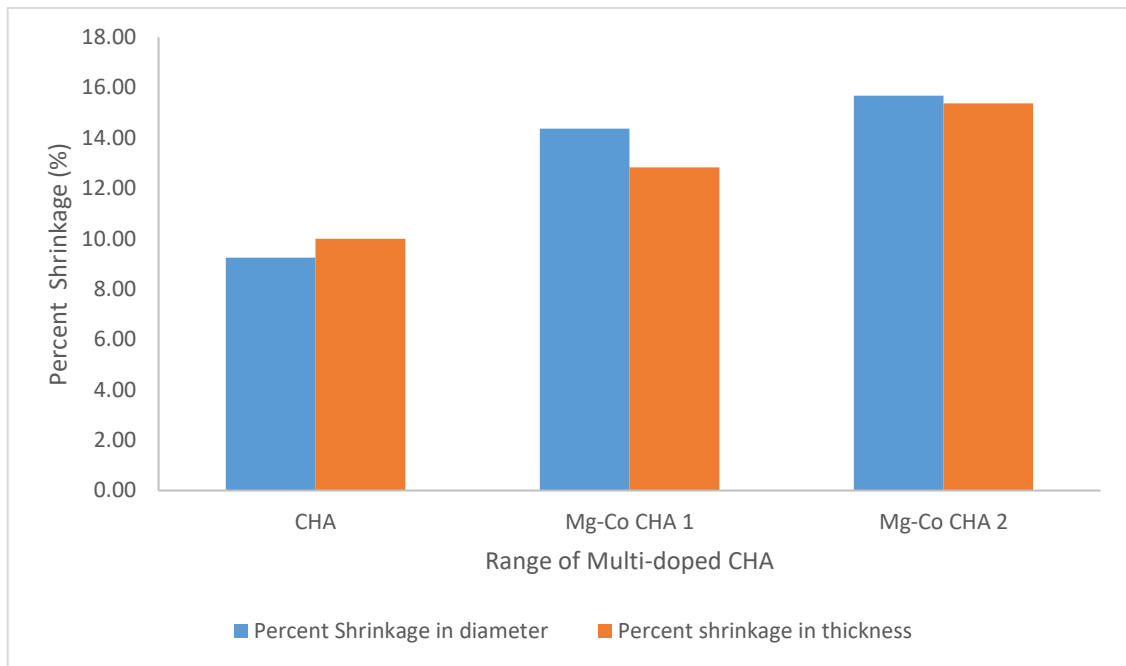


**Figure 4.13:** Percent of shrinkage in diameter and thickness of CHA, Mg-Co CHA 1 and Mg-Co CHA2.

#### 4.4.4 Density and Porosity Measurement

Porosity is removed from ceramic green body when samples undergo sintering process, causes the samples to fully densify. As porosity removed, the samples also experience reduction in terms of its surface area. As surface area was reduced, there will be change in density and causes stress to develop. As the samples undergo sintering process, samples will decrease in volume and increase in density (Ring & Ring, 1996).

Thus, it can be said that the relative density and apparent porosity result of the sample co-related with the result of shrinkage. Where, the highest density should experience the highest shrinkage, with lowest porosity. Based on the relative density and apparent porosity result shows in Table 4.15, Mg-Co 2 has the highest relative density with the lowest porosity, co-related with shrinkage result, the highest percentage of shrinkage was Mg-Co 2. It is observed that sample with highest density also experience the highest shrinkage. This can be explained by solid state sintering reaction, where the pores shrink continuously and may disappear altogether, resulting on a dense body.

**Table 4.16:** Average apparent porosity, bulk density, powder density and relative density for (a) CHA (b) Mg-Co CHA 1 and (c) Mg-Co CHA 2.

(a)

	<b>Reading 1</b>	<b>Reading 2</b>	<b>Reading 3</b>	<b>Average</b>
<b>Apparent Porosity (%)</b>	46.52	51.61	48.03	<b>48.720</b>
<b>Bulk Density</b>	1.64	1.47	1.58	<b>48.720</b>
<b>Powder Density</b>				<b>2.7158</b>
<b>Relative Density</b>	60.3874	54.1277	58.1781	<b>57.564</b>

(b)

	<b>Reading 1</b>	<b>Reading 2</b>	<b>Reading 3</b>	<b>Average</b>
<b>Apparent Porosity (%)</b>	42.88	43.07	39.1	<b>41.683</b>
<b>Bulk Density</b>	1.74	1.76	1.9	<b>41.683</b>
<b>Powder Density</b>				<b>2.554</b>
<b>Relative Density</b>	68.1284	68.9115	74.3931	<b>70.478</b>

(c)

	Reading 1	Reading 2	Reading 3	Average
<b>Apparent Porosity (%)</b>	28.15	29.16	26.48	<b>27.930</b>
<b>Bulk Density</b>	2.22	2.17	2.24	<b>27.930</b>
<b>Powder Density</b>				<b>2.594</b>
<b>Relative Density</b>	85.5821	83.6546	86.3531	<b>85.197</b>

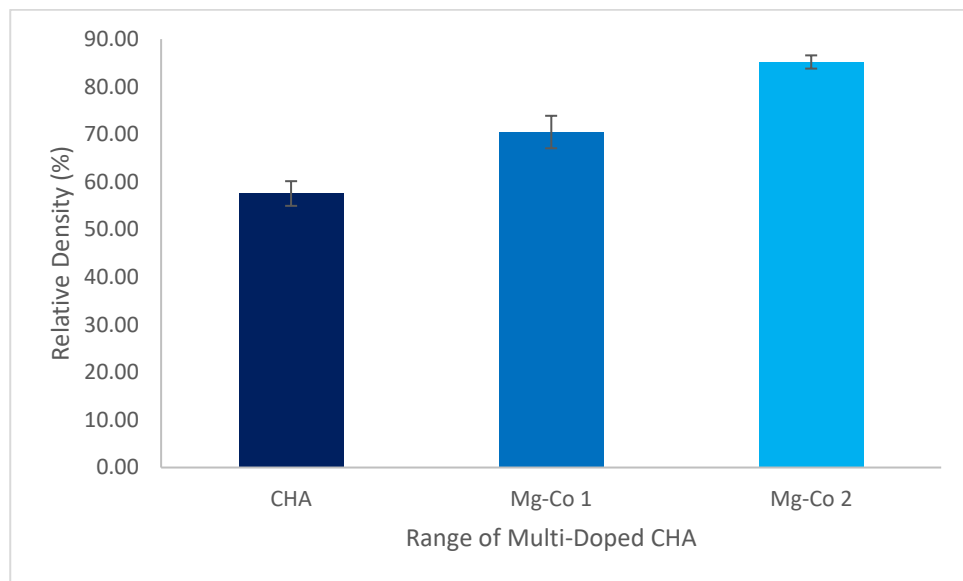


**Figure 4.14:** Relative density of CHA and multi-doped CHA.

#### 4.4.5 Diametral Tensile Strength

Diametral Tensile Strength (DTS) data shows the tensile strength that can be withstand for each sample. Results shows similar trend with shrinkage and density and porosity result, where the highest was Mg-Co 2, followed with Mg-Co 1 and the lowest is CHA. Based on the highest value of tensile strength, which is 3.85 MPa by Mg-Co 2, this amount is similar with amount of tensile strength by cervical vertebrae, 3.1 MPa (Bandyopadhyay et al. 2006). Thus, it can be used for bone substitution for cervical vertebrae.

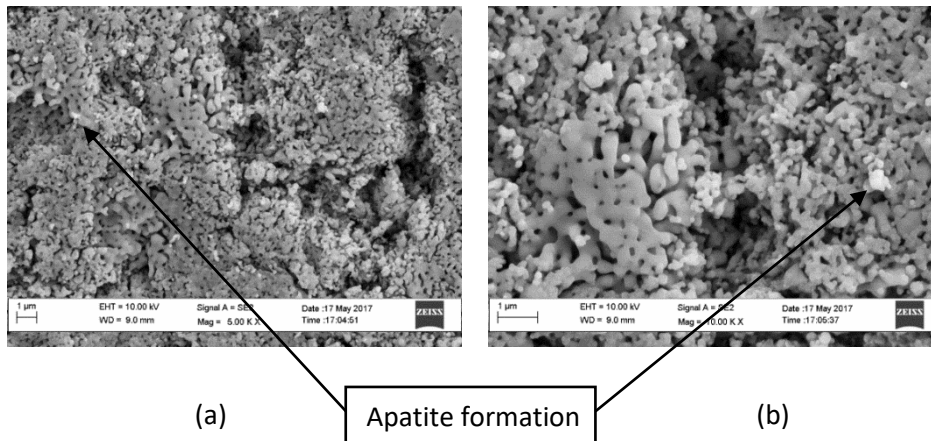
**Table 4.17:** Tensile strength of sintered CHA and multi-doped CHA.

	<b>CHA</b>	<b>Mg-Co CHA 1</b>	<b>Mg-Co CHA 2</b>
<b>Tensile Strength (MPa)</b>	2.85	3.65	3.85

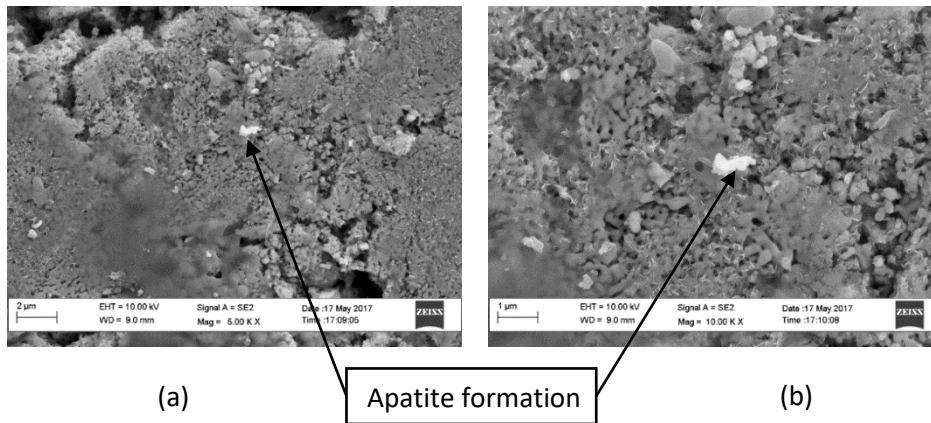
#### **4.4.6 Field Emission Scanning Electron Microscopy/ Energy Dispersive X-Ray**

Field Emission Scanning Electron Microscopy (FESEM) was conducted to analyze the formation of apatite layer for sample that undergo bioactivity test (*in vitro*), where dense CHA and multi-doped CHA were soaked in Simulated Body Fluid (SBF) for seven days and the temperature was kept at 37°C. After seven days, the samples were taken out, washed carefully with deionized water and dried. Drying at 37°C in oven were done before coat with gold and underdo SEM analysis to ensure that the samples were completely dry.

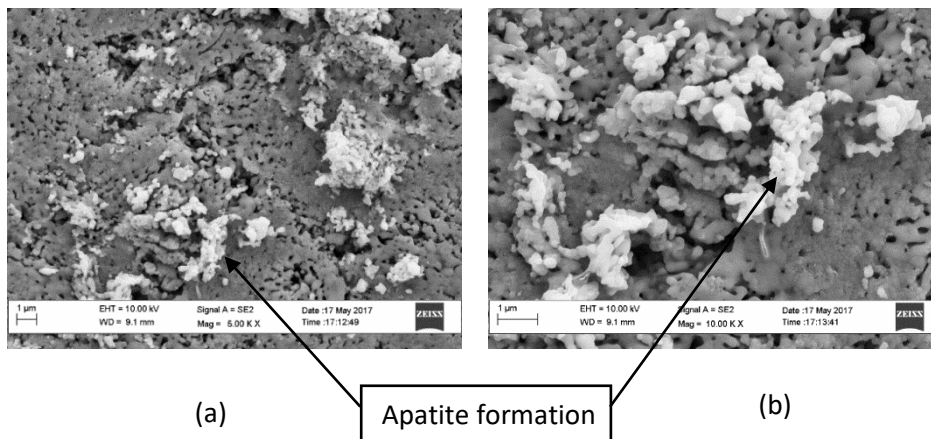
Interaction between the sample and ions from SBF solution causes formation of apatite layer on the surface of the sample. The formation of the apatite layer on the surface has a beneficial effect on cell adhesion during implantation. Thus, it has high possibility for bone to regenerate if being implanted (González Ocampo et al., 2016). Figure 4.14 to 4.16 showed a small formation of apatite layer on the surface of the samples. CHA has the highest amount of apatite layer form, compared to Mg-Co CHA 1 and Mg-Co CHA 2. Meanwhile, Mg-Co CHA 2 produce more apatite layer when compared to Mg-Co CHA 1. It is confirmed that apatite layer were formed as apatite layer shape that were formed were distinct compare with sample.



**Figure 4.15:** Surface morphology of CHA based under 5000x and 10000x magnification.

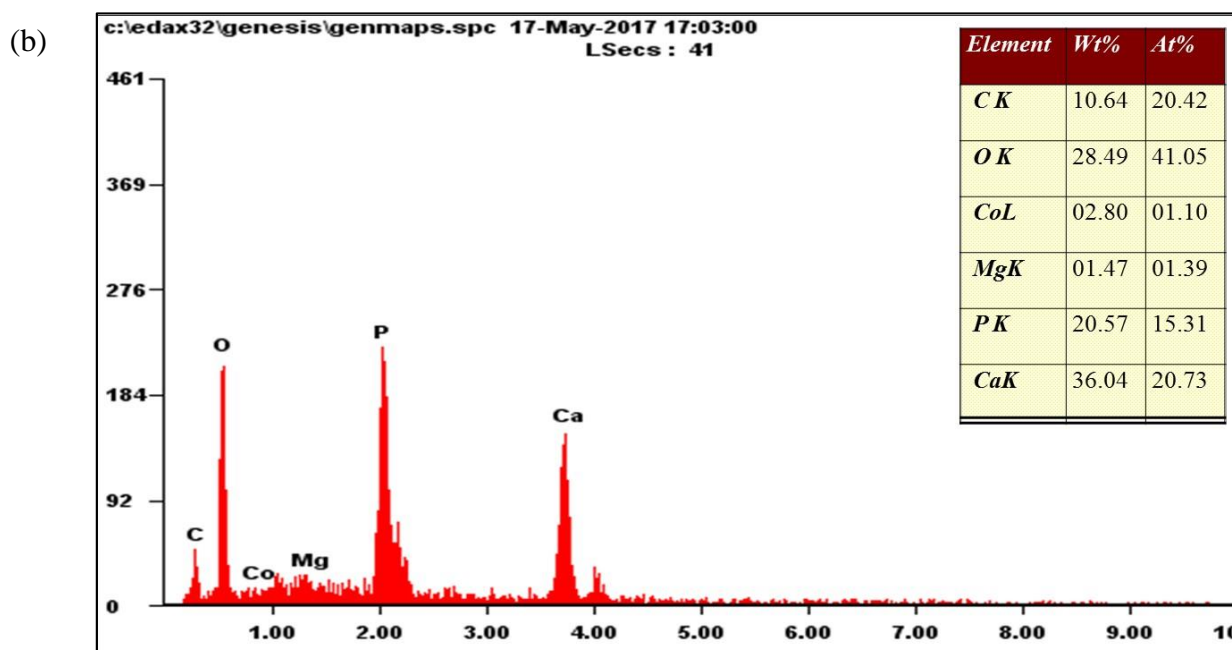
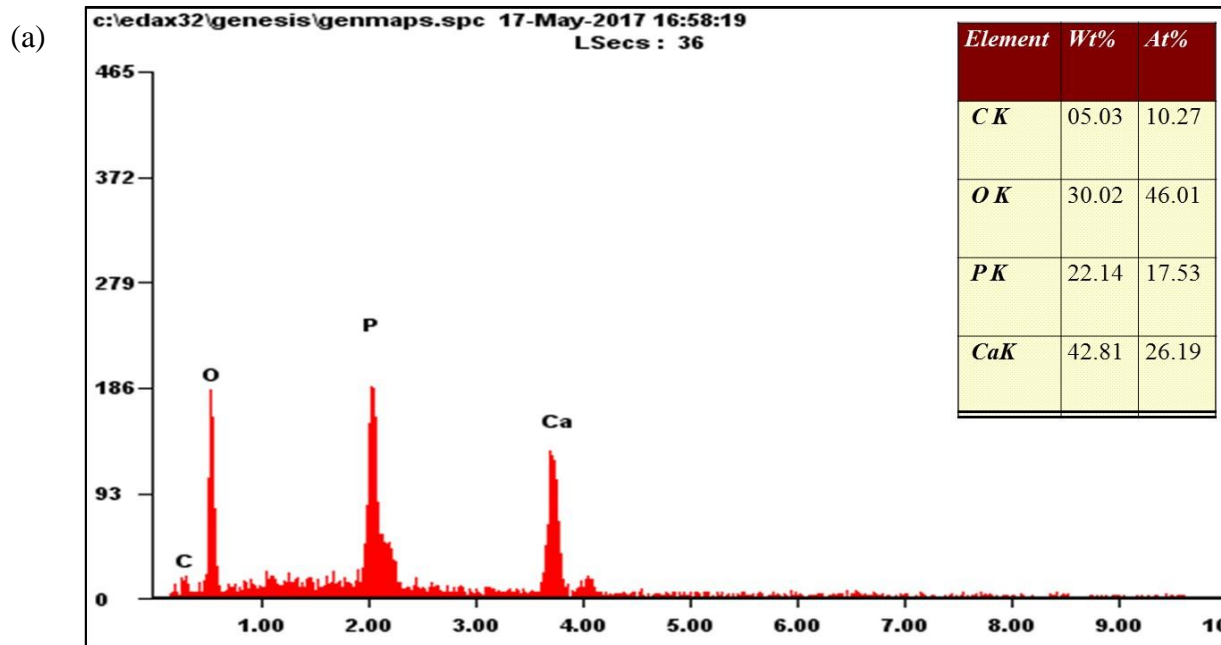


**Figure 4.16:** Surface morphology of Mg-Co CHA1 based under (a) 5000x and (b) 10000x magnification.



**Figure 4.17:** Surface morphology of Mg-Co CHA2 based under (a) 5000x and (b) 10000x magnification.

Energy Dispersive X-Ray (EDX) was conducted to evaluate the element of layer form, either the doping element were present or not. It is prove that the materials has been substitute into CHA structure perfectly, as dopant materials were present throughout the study.



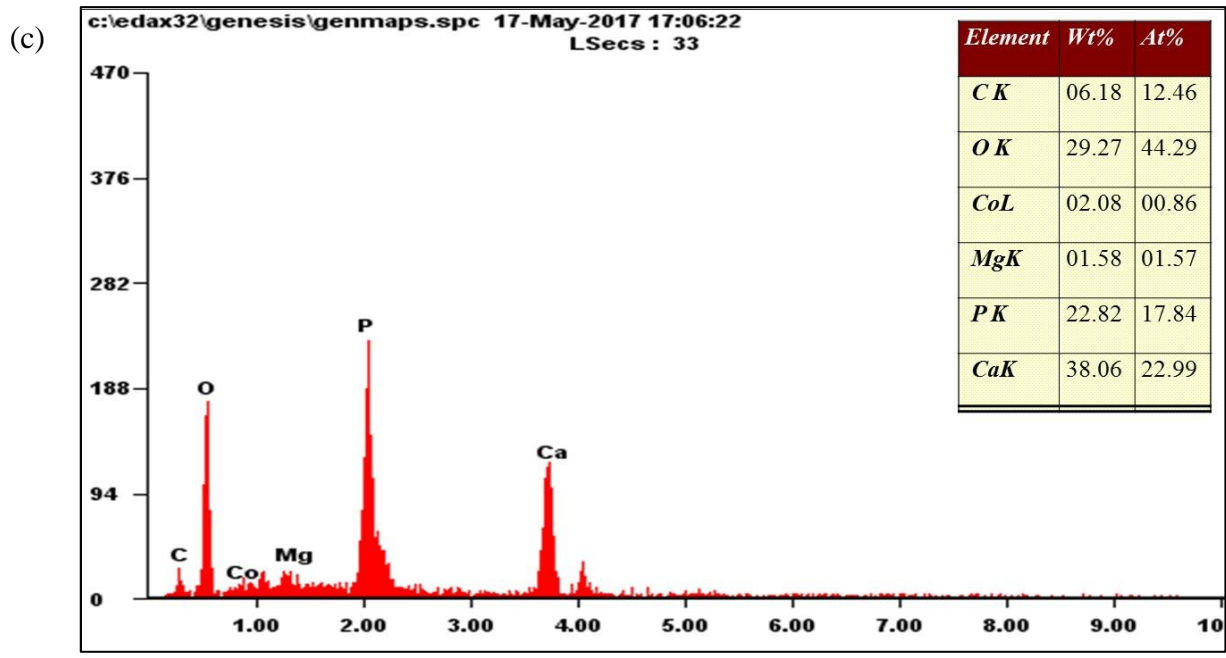


**Figure 4.18:** EDX result of (a) CHA (b) Mg-Co CHA 1 (c) Mg-Co CHA 2.

## CHAPTER 5

### CONCLUSION AND RECOMMENDATION

#### 5.1 Conclusion

In this study, Carbonated Hydroxyapatite (CHA) and multi-doped CHA were synthesized via nanoemulsion method through direct pouring technique at the first stage. Then, followed by characterizations of the produced CHA powders and multi-doped CHA powders at second stage. Analysis of the results obtain from characterizations at second stage showed that all of multi-doped CHA were successfully doped with magnesium and cobalt, purely HA based with single phase and a B-type CHA. Then, Mg-Co CHA 1 and Mg-Co CHA 2 powders were selected as the optimum compositions based on the amount of cobalt and magnesium for each compositions, as cobalt content should not present in high amount as it can cause toxicity issues.

The CHA, Mg-Co CHA 1 and Mg-Co CHA 2 powders were then used in making of pellets via dry pressing method as these were the optimum compositions for the third stage. Then, followed by characterizations of the dense CHA and dense multi-doped CHA at final stage. Analysis of the results obtain from characterizations at final stage showed that all the dense multi-doped CHA remained as pure HA based, single phase and B-type CHA. It also found that doping has improved physical, mechanical and biological properties in particularly encouraging rigid apatite layer formation as compared to pure CHA. Based on SEM results, apatite layer can be observed on the surface for all samples. Among the tested samples, Mg-Co CHA 2 shows the highest amount of apatite layer formation. Therefore, Mg-Co CHA 2 sintered samples was chosen to be the optimum composition as it has good physical, mechanical and biological properties in comparison to Mg-Co CHA 1.

## 5.2 Recommendation for Future Work

The current study required further improvement for future work, in order to improve the outcome of this study, which is to produce multi-doped CHA to be used as biomedical application. Improvement that can be done for future work are:

- 1) Used of different composition of cobalt to ensure that it can be detected during XRF analysis.
- 2) Conducting Transmission Electron Microscope (TEM) analysis to estimate the actual particle size and shape.
- 3) Used of dispersant to prevent powders from aggregating in order to get a better dispersed particles, Ethanolamine, citric acid and polyethylene glycol are an example of dispersants that can be used in future work.
- 4) Further study in term of biological properties, where conducting both *in-vitro* and *in-vivo* studies, to strengthen the outcome of the study.

## REFERENCES

### Journals

Baba Ismail, Y.-M. & Mohd Noor, A.-F., 2011. Effect of a Novel Approach of Sintering on Physical Properties of Carbonated Hydroxyapatite. *Journal of Materials Science and Engineering B*, 1(October), pp.157–163.

Baba Ismail, Y.M. et al., 2017. Development of multisubstituted hydroxyapatite nanopowders as biomedical materials for bone tissue engineering applications. *Journal of Biomedical Materials Research - Part A*, pp.1–11.

Bandyopadhyay, A. et al., 2006. Calcium phosphate-based resorbable ceramics: Influence of MgO, ZnO, and SiO<sub>2</sub> dopants. *Journal of the American Ceramic Society*, 89(9), pp.2675–2688.

Bang, L.T., Long, B.D. & Othman, R., 2014. Carbonate hydroxyapatite and silicon-substituted carbonate hydroxyapatite: Synthesis, mechanical properties, and solubility evaluations. *The Scientific World Journal*, 2014(October 2016).

Barinov, S.M. et al., 2006. Carbonate release from carbonated hydroxyapatite in the wide temperature range. *Journal of Materials Science: Materials in Medicine*, 17(7), pp.597–604.

Batra, U. & Kapoor, S., 2016. Ionic Substituted Hydroxyapatite Scaffolds Prepared by Sponge Replication Technique for Bone Regeneration. , 6, pp.18–24.

Best, S.M. et al., 2008. Bioceramics : Past , present and for the future. , 28, pp.1319–1327.

Boanini, E., Gazzano, M. & Bigi, A., 2010. Ionic substitutions in calcium phosphates synthesized at low temperature. *Acta Biomaterialia*, 6(6), pp.1882–1894.

Boneva, R.S., Folks, T.M. & Louisa, E., 2001. Infectious Disease Issues in Xenotransplantation Infectious Disease Issues in Xenotransplantation. , 14(1), pp.1–14.

Chevalier, J. & Gremillard, L., 2009. Ceramics for medical applications : A picture for the next 20 years. , 29, pp.1245–1255.

Combes, C., Cazalbou, S. & Rey, C., 2016. Apatite Biominerals. *Minerals*, pp.1–25.

Dorozhkin, S. V. & Epple, M., 2002. Biological and medical significance of calcium phosphates. *Angewandte Chemie - International Edition*, 41(17), pp.3130–3146.

Egawa, S. et al., 2014. Growth and differentiation of a long bone in limb development, repair and regeneration. *Development Growth and Differentiation*, 56(5), pp.410–424.

Eliasz, N. & Metoki, N., 2017. Calcium Phosphate Bioceramics : A Review of Their

History, Structure, Properties, Coating Technologies and Biomedical Applications.

González Ocampo, J.I., Escobar Sierra, D.M. & Ossa Orozco, C.P., 2016. Porous bodies of hydroxyapatite produced by a combination of the gel-casting and polymer sponge methods. *Journal of Advanced Research*, 7(2), pp.297–304.

Guo, L., Huang, M.E.I. & Zhang, X., 2003. Effects of sintering temperature on structure of hydroxyapatite studied with Rietveld method. , 4, pp.817–822.

Hanson, E.T. et al., 2002. Third-Generation Biomedical Materials. , 295(February), pp.1014–1017.

Kehoe, S. & Eng, B., 2008. Optimisation of Hydroxyapatite ( HAp ) for Orthopaedic Application via the Chemical Precipitation Technique By. *Rheology*, (September).

Kokubo, T. & Takadama, H., 2006. How useful is SBF in predicting in vivo bone bioactivity? *Biomaterials*, 27(15), pp.2907–2915.

Kulanthaivel, S. et al., 2015. Improving the osteogenic and angiogenic properties of synthetic hydroxyapatite by dual doping of bivalent cobalt and magnesium ion. *Ceramics International*, 41(9), pp.11323–11333.

Kumar, G.S. et al., 2012. Synthesis, characterization and in vitro studies of zinc and carbonate co-substituted nano-hydroxyapatite for biomedical applications. *Materials Chemistry and Physics*, 134(2–3), pp.1127–1135.

Landi, E. et al., 2006. Biomimetic Mg- and Mg<sub>2</sub>CO<sub>3</sub>-substituted hydroxyapatites: synthesis characterization and in vitro behaviour. *Journal of the European Ceramic Society*, 26(13), pp.2593–2601.

Laurencin, D. et al., 2011. Magnesium incorporation into hydroxyapatite. *Biomaterials*, 32(7), pp.1826–1837.

Lima, P.A.L. et al., 2013. Preparation, characterization and biological test of 3D-scaffolds based on chitosan, fibroin and hydroxyapatite for bone tissue engineering. *Materials Science and Engineering C*, 33(6), pp.3389–3395.

Mickiewicz, R.A., 2001. Polymer-calcium phosphate composites for use as an injectable bone substitute. , (June).

Monika, Š., 2015. Substituted hydroxyapatites for biomedical applications : A review Substituted hydroxyapatites for biomedical applications : A review. , (May).

Parthiban, S.P. et al., 2011. In vitro study of carbonated hydroxyapatite compacts prepared by double-step hydrothermal method. *IOP Conference Series: Materials Science and Engineering*, 18(19), p.192008.

Ramay, H.R. & Zhang, M., 2003. Preparation of porous hydroxyapatite scaffolds by combination of the gel-casting and polymer sponge methods. *Biomaterials*, 24(19), pp.3293–3302.

- Ring, T.A. & Ring, T.A., 1996. Sintering and Finishing. *Fundamentals of Ceramic Powder Processing and Synthesis*, pp.777–780.
- Sadat-shojai, M. et al., 2013. Acta Biomaterialia Synthesis methods for nanosized hydroxyapatite with diverse structures. *Acta Biomaterialia*, 9(8), pp.7591–7621.
- Serre, C.M. et al., 1998. Influence of magnesium substitution on a collagen-apatite biomaterial on the production of a calcifying matrix by human osteoblasts. *Journal of Biomedical Materials Research*, 42(4), pp.626–633.
- Shepherd, J.H., Shepherd, D. V. & Best, S.M., 2012. Substituted hydroxyapatites for bone repair. *Journal of Materials Science: Materials in Medicine*, 23(10), pp.2335–2347.
- Ślósarczyk, A., Paszkiewicz, Z. & Paluszkiwicz, C., 2005. FTIR and XRD evaluation of carbonated hydroxyapatite powders synthesized by wet methods. *Journal of Molecular Structure*, 744–747(SPEC. ISS.), pp.657–661.
- Tan, G., 2015. Fourth-generation biomedical materials. *Biochemical Pharmacology*, (December), pp.10–12.
- Teixeira, S. et al., 2010. In vivo evaluation of highly macroporous ceramic scaffolds for bone tissue engineering. *Journal of Biomedical Materials Research - Part A*, 93(2), pp.567–575.
- Vallet-regí, M., 2010. Evolution of bioceramics within the field of biomaterials. , 13, pp.174–185.
- Wang, M., 2003. Developing bioactive composite materials for tissue replacement. , 24(October 2002), pp.2133–2151.
- Whited, B.M. et al., 2005. Osteoblast Response to Zirconia-Hybridized Pyrophosphate Stabilized Amorphous Calcium Phosphate Osteoblast Response to Zirconia-Hybridized Pyrophosphate Stabilized Amorphous Calcium Phosphate.
- Wong, W.Y. & Mohd Noor, A.-F., 2016. Synthesis and Sintering-wet Carbonation of Nano-sized Carbonated Hydroxyapatite. *Procedia Chemistry*, 19, pp.98–105.
- Wu, Z.Y., 2010. Development of novel 3D porous melt-derived bioactive glass scaffolds. , (September).
- Zhou, W.Y. et al., 2008. Synthesis of carbonated hydroxyapatite nanospheres through nanoemulsion. *Journal of Materials Science: Materials in Medicine*, 19(1), pp.103–110.
- Zilm, M., Thomson, S.D. & Wei, M., 2015. A comparative study of the sintering behavior of pure and manganese-substituted hydroxyapatite. *Materials*, 8(9), pp.6419–6436.